LAWRENCE
LIVERMORE
NATIONAL
LABORATORY

LLNL-TR-645701

Particle Simulation of High-Intensity X-Ray Laser Interaction

R. M. More

November 5, 2013

Disclaimer

This work performed under the auspices of the U.S. Department of Energy by Lawrence Livermore National Laboratory under Contract DE-AC52-07NA27344.

Particle Simulation of High-Intensity X-Ray Laser Interaction

An LLNL LDRD Feasibility Study Project

SUMMARY REPORT:
GOAL,
METHODS,
RESULTS
&
FUTURE POSSIBILITIES

Richard M. More
28 October, 2013

Report of work performed under subcontract B604796

Particle Simulation of High-Intensity X-Ray Laser Interaction
LLNL LDRD Feasibility Study Project - FINAL REPORT -
Subcontract B604796 **Richard M. More**

CONTENTS

1.) OVERVIEW and SUMMARY

This Feasibility Study Project began with two goals:

1.) Develop the techniques needed to combine molecular dynamics (MD) particle simulation with atomic kinetics described by a "Collisional-Radiative" (CR) model.[1] Investigate the computational requirements and possible physics improvements to the calculation, especially quantum corrections. The feasibility question is: "*Can we do the calculation and will it run fast enough to be useful?*"

2.) Test the calculations against X-ray Free-electron Laser interaction experiments on solid Fe targets performed by Prof. H. Yoneda et al. at the SACLA XFEL facility in the SPring-8 laboratory in Harima, Japan.[2] The remarkable parameters of the experiments are:

X-ray photon energy = 7.1 keV
X-ray pulse length = 10 femtoseconds
X-ray intensity in the range 10^{19} to 10^{20} Watts/cm^2

The extraordinary high intensity (about 1000 times the best published SLAC-LCLS result) is obtained by use of high-quality reflective (Kirkpatrick-Baez) X-ray focusing optics and by careful control of vibrations from equipment in the target room.
The feasibility questions are: "*Will the theory be anything like the experiments?*" and "*Can the calculations be a useful guide to future experiments, either at SACLA or LCLS ?* "

In new experiments (Summer, 2013) the SACLA XFEL has been used as a pump laser for saturated X-ray lasing from K_α transitions (8 keV) of Cu targets. We describe these exciting experiments below[3]. This new experimental situation has given us a strong feeling of *mission creep* - we want to predict the next round of experiments - and a great increase in our ambitions for this work.

2.) METHODS: MD + CR

For this project we wrote 5 new computer codes. Here we give a brief sketch of the computational techniques used in these codes.

The method of molecular dynamics particle simulation was invented in Livermore in the 1950's as an early scientific application of large digital computers.[4] MD has been used since then to study dense fluids of hard spheres or point charges to learn about their thermodynamic behavior and phase transitions. Our basic idea is that the particles used for the simulation can have excited states and make transitions or reactions, like real atoms or molecules in hot matter, and this greater realism is within the reach of modern workstation computers[1].

The Collisional-Radiative model (CR model) for atomic kinetics has been used to analyze experimental spectra from astrophysics and from laboratory experiments on magnetic fusion. British scientists (Bates, Kingston and McWhirter, Seaton and others) took an early lead, based on their strength in atomic data[5,6,7,8]. In the 1980's Livermore assembled strong research teams and powerful CR computer codes for various purposes, especially for X-ray laser research.

The idea of combining MD with CR has motivated several research groups. A Livermore group led by F. Graziani based their work on an existing particle simulation code (DDCmd). This author worked with them during the years 2005-2010, learning computational techniques and making an independent assessment of priorities.[9,10,11] The Graziani group has focused attention on experiments that use LCLS X-rays as *diagnostics* of plasmas heated to WDM temperatures by ordinary lasers.[12] For the most part, they decided to develop MD simulations in which the electrons are treated as classical particles and use pseudopotentials to try to improve the low-temperature electron correlation behavior. This author has explored a different path, treating the electrons as a fluid (as in the usual plasma CR model) and looking at higher temperatures where electron correlations are (normally) less important. Treating the electrons as a fluid has the practical advantage of making possible much larger computational time-steps, which in turn made it possible perform 20 psec fusion ignition simulations of self-heating DT fuel,[1,13] or the 20 fsec simulations of XFEL interactions reported here.

At the CEA Laboratory in Bruyeres le Chatel, Gerald Faussurier and Christophe Blancard also plan to develop a CR+MD simulation code. They have discussed the difficulties of reconciling the treatments of bound and free electrons when the electrons are treated as classical particles[14].

MD + CR particle simulations are sharply different from the well-known and well-developed method of "Quantum Molecular Dynamics" (QMD) which describes equilibrium (LTE) conditions, normally at relatively low temperatures[15]. The QMD method combines particle ions with a density-functional treatment of electrons in thermal equilibrium. MD + CR is appropriate to study the transient, non-equilibrium behavior of violently heated plasmas in which the atomic states and/or ion velocities do not have equilibrium (Maxwell-Boltzmann) distributions.

X-FEL Experiments

The Japanese XFEL experiments are performed on an electron linac named SACLA (apparently pronounced "Sakura" = Cherry blossom) located at the SPring-8 light-source facility in Harima, Japan[16]. SACLA is about ¼ mile long and has an undulator generating an X-ray Free Electron laser (XFEL). It is much smaller than LCLS because it uses high-frequency electronics ("C-band"). SACLA produces about ½ millijoule of X-rays per pulse, tunable, with photon energies of 7 -10 keV for the experiments discussed here. The X-ray pulse duration is 10 fsec and the rep-rate is about 20 Hz. These parameters are not amazing, but by using two-stage Kirkpatrick-Baez focusing optics, the X-rays are *focused to a 50 nanometer focal spot.*

The spot-size is confirmed by imaging wire arrays placed upstream from the best focus. The focused energy is probably only one percent of the SACLA output(~ 20 microjoules), but it reaches intensities up to 10^{20} Watts per cm^2 on and inside the target.

Such high intensities were achieved with ultra-short pulse visible lasers ("petawatt lasers")[17] but never before with hard X-rays. The intensity quoted is about 1000 times brighter than the best published result from LCLS. Our calculations confirm the claimed high intensities because we find the observed bleaching phenomenon does not occur for Fe at lower X-ray intensities.

Focal spot geometry

In the SACLA experiments, Fe foils of 10, 20 micron thickness are irradiated by the XFEL, which effectively digs a thin tunnel of heated material through the foil. The focal spot size is about 50 nanometers diameter but the post-shot damage hole is about 1 micron in radius. At lower intensity (up to, say 10^{18} Watt/cm^2) the x-rays are simply absorbed according to the cold-matter absorption coefficient, but above that intensity enough K-shell holes are produced to significantly reduce the absorption and increase the transmission. This is *bleaching* of the Fe foil.

Although the Fe experiment is interesting in itself, it has special features which simplify the requirements for modeling, and our computer code will ultimately want to handle more general situations. A first special feature is the short X-ray pulse duration. There is not much atomic motion during 10-20 femtoseconds, so the MD part of our calculation is not heavily tested. Second, the SACLA experiments do not yet have high-resolution spectroscopy, so the interesting effects of transient ionization on the line profiles are not yet measured. Our computer calculations can suggest or predict future experiments with better diagnostics. A third special feature is the "one-way" energy transfer: X-ray energy enters the target atoms as K-shell ionization and then cascades to lower energies without many back-transitions. This is a simplification for atomic modeling. We have tried to exploit these simplifying features. It is obviously a good strategy to develop a new computational model in the context of a specific experiment, taking advantage of any simplifying features. One can extend the code capabilities later.

3.) RESULTS from this project (brief summary):

1.) We wrote five new computer codes for this project. These are codes which were used to perform calculations and are not polished user-friendly software tools.

2.) We performed Collisional-Radiative modeling with molecular dynamics (CR + MD) for 20,000 computational Fe atoms. The calculations predict XFEL bleaching of a 20 μ foil at intensities ~ 2 10^{19} W/cm^2 (= peak intensity of a 10 fsec gaussian pulse). That is very close to the (unpublished) experimental measurement. (Section 5)

3.) Using the CR + MD code, we predict that the K_α line (at 6.4 keV for Fe) will show gain at high pump intensity. For a pump peak intensity of 10^{19} W/cm^2 we predict gain of about 2.2 10^4 cm^{-1} for the Fe K_α transition. The most recent experiments at SACLA

indeed show similar gain for the corresponding K_α transition in Cu at 8 keV. With this experiment, one has a high-gain (saturated) X-ray laser at 8 keV, pumped by the XFEL. In comparison, an LCLS experiment performed last year by a Livermore experimental group observed lasing in Neon gas at 0.8 keV.[18] (section 5)

Our code also predicts sub-keV gain, for example for the Fe core-hole transition 2p --> 3s we predict a gain of 1.8 10^3 cm^{-1} at 0.627 keV, occuring simultaneously with the stronger gain on the K_α transition.

4.) A Schroedinger + MD code was developed to explore quantum atomic phenomena that a CR model cannot encompass. This code solves the density-matrix equation of motion and calculates line profiles by the Kubo-Baranger method. The code was tested by calculating Stark profiles for a gas of 300 hydrogen atoms moving in the presence of a low density of charge +1 impurity ions. This calculation could be used to perform a more rigorous treatment of *ion dynamical* effects in plasma line broadening[5,6,7]: the electric field seen by each hydrogen emitter changes magnitude and direction as the atom moves. The calculation needs certain improvements before it will be a realistic plasma line-broadening calculation, but the MD plus Schroedinger calculation is working. (Section 8)

5.) We developed an analytic calculation for the effect of collisions upon super-radiance in few-atom systems. Rapid collisions are found to suppress super-radiance in the same way as line-broadening reduces the XRL gain. (Section 7)

Future potential applications of MD+CR

We list here potential future tests and applications of the MD + CR code family.

1.) An experiment on aluminum at LCLS provides well-diagnosed spectra and will be an excellent test for MD + CR modeling[19]. The LCLS diagnostics are much more elaborate than those deployed in SACLA. (This experiment observed bleaching of Al.)

2.) The LCLS Neon XFEL-pumped XRL experiment mentioned above can also provide a test of the MD + CR code[18]. Both these LCLS experiments are done with longer pulses and are thus more sensitive to ion motion.

3.) New XFEL systems are under construction in Hamburg, Germany, in Pohang, South Korea, and at LCLS where an upgrade is underway. The MD+CR method can provide unique modeling tool for future experiments in any of these facilities.

4.) The method of MD + CR offers a new approach for calculations of plasma opacity, especially for non-LTE plasmas. The special benefit of the MD+CR combination is the ability to use different line-broadening for different atoms (ions) in the calculation, depending on the local environment of each atom. True opacity calculations would be very demanding computationally but would be feasible on large computers.

5.) The combination of MD with the Schroedinger equation seems ideally suited to simulation of laser cooling and trapping phenomena. In that case a small number of real atoms are manipulated by precisely tuned lasers that only interact with those few atoms having the right Doppler shift. In this one case, the MD might be able to treat as many atoms as are present in the experiment.

6.) Dr. F. Wang of the Beijing Astronomical Observatory (NOAC) has repeatedly drawn our attention to the possible application of MD + CR modeling for astrophysics, especially for radiation from compact stars with large magnetic fields or for radiation emitted by active galactic nuclei.

7.) There are many uses of different computer models (including versions of MD) for study of chemical reactions, but a preliminary literature search convinces this author that there remain interesting possibilities for modeling detonation waves, especially those in which radiation emission and energy transfer play an important role. For example, the rapid explosion of hydrogen-oxygen gas mixtures may be enabled by propagation of UV radiation which dissociates O_2 or H_2 molecules and provides the seeds for chain-branching reactions. If this is true it would be possible to inhibit the explosive reaction by introducing a high-opacity impurity gas --- something that could have saved trillions of Japanese yen in Fukushima. MD studies of this idea are surely cheaper and safer than Laboratory experiments.

8.) Closely analogous, the method of MD + particle reactions has been used to study fusion ignition experiments. The fusion physics accessible to MD simulations concerns non-Maxwellian ion velocity distributions and their effects[13].

4.) FUTURE POSSIBILITIES: XFEL --> XRL pump radiation

The latest round of SACLA experiments uses the XFEL as a pump for a saturated inner-shell X-ray laser. The laser medium is solid-density Cu. There is no need for difficult pulse-control or timing multiple pulses against the expansion-time. The gain medium has relatively low temperature, and the XFEL pulse length is very short[3].

Importance to Livermore Lab

Throughout the 1980's, Livermore had a pioneering research program in X-ray laser science. Livermore produced the World's first Laboratory soft X-ray laser (80 eV photons) and pioneered many improvements in that technology. Livermore scientists proposed key ideas for inner-shell lasers[20]. Livermore scientists held many meetings to discuss the marvelous potential applications of X-ray lasers, but in most cases those applications needed harder X-rays (in the keV range) and shorter pulses (to avoid exploding biological molecules by the X-ray probe). Now all those applications are within reach -- of Japanese scientists in Harima, near Osaka. Will this be another tragic example of pioneering research done in US, exploitation done overseas?

People skeptical of the possibilities for important applications of X-ray lasers should recall the history of visible lasers. For many years, laser technology was derided

as "a solution looking for a problem" but today all our digital technology is based on one or another application of lasers. From hard disk to printer this document is produced by lasers. It took perhaps 50 years from pure research to the time when commercial lasers are riding in your automobile and even in your pocket. The widespread use of lasers makes our modern world a second "*Age of Lumière*".

X-ray lasers will offer unprecedented improvements in medical imaging, precision measurement of small objects, perhaps holography of proteins or other molecules, possibly fabrication of new nanostructures (today Yoneda's XFEL makes holes with a one micron diameter through a 20 micron Fe foil). Borrowing from the symbol of crossed cannons at the gate of the Ecole Polytechnique, one can say we are entering "*l'Age de l'X*". The US and the Livermore Lab should not look on passively as this train leaves the station.

A specific proposal

During the coming year, we would like to help organize a group of Livermore scientists to vigorously perform XFEL experiments on the LCLS upgrade during 2015. Because we will have the unique modeling capability outlined in this report, our team can design better experiments than any other research group.

REFERENCES

1.) R. More and F. Wang, "**Molecular dynamics with atomic transitions and nuclear reactions**", 24th IUPAP Conference on Computational Physics (IUPAP-CCP 2013), Journal of Physics Conference Series **454**, 012027 (2013).

2.) H. Yoneda and 9 co-authors, "**Nonlinear optics for multi-keV X-ray lasers**", preprint.

3.) H. Yoneda et al., unpublished. Dr. Yoneda showed the recent experimental results in a LLNL seminar on August 14, 2013, and we discussed further with him in off-site meetings.

4.) B. Alder and T. Wainwright, J. Chem. Phys. **27**, 1208 (1957); J. Chem. Phys. **31**, 459 (1959).

5.) H. Griem, **Principles of Plasma Spectroscopy**, Cambridge, 1997.

6.) D. Salzmann, **Atomic Physics in Hot Plasmas**, Oxford, 1998.

7.) T. Fujimoto, **Plasma Spectroscopy**, Oxford, 2004.

8.) R. More, T. Kato, S. Libby and G. Faussurier, JQSRT 71, 2001.

9.) R. More, F. Graziani, J. Glosli and M. Surh, High Energy Density Physics **6**, 29 (2010).

10.) J. Glosli, F. Graziani, R. More, M. Murillo, F. Streitz and M. Surh, J. Phys. **A 42**, 214030 (2009).

11.) R. More, M. Goto, F. Graziani, P. Ni and H. Yoneda, Plasma and Fusion Research **5**, S2008 (2010).

12.) S. P. Hau-Riege, J. Weisheit, J. Castor, R. London, H. Scott and D. Richards, "**Modeling quantum processes in classical molecular dynamics simulations of dense plasmas**", New Journal of Physics **15**, 015011 (2013).

13.) R. More, "**Particle Simulation Code for Fusion Ignition**", in Nuclear Instruments and Methods **A**, 2013.05.067 (2013).

14.) Drs. Gerald Faussurier and Christophe Blancard, CEA-BLC, *en direct* (personal communication).

15.) A. Mattsson, P. Schultz, M. P. Desjarlais, T. Mattsson and K. Leung, "**Designing meaningful density functional theory calculations in materials science -- a primer**", in Modeling Simulations in Material Science and Engineering **13**, R1 (2005).

16.) Pictures of the machine and laboratories can be found on the web using the search-words "SACLA, Harima, SPring-8". The name "SACLA" has a confusing similarity to "SLAC", probably not deliberate. It is pronounced "Sakura" because of a limitation of the Katakana alphabet: every consonant (except "n") must be followed by a vowel in that alphabet.

17.) See **Science of Super-strong Field Interactions**, Ed. by K. Nakajima and M. Deguchi, AIP Conference Proceedings, vol. 634 (2002).

18.) N. Rohringer, D. Ryan, R. London and nine other co-authors, "**Atomic Inner-shell X-ray laser at 1.46 nanometers pumped by an X-ray free-electron laser**", Nature **481**, 488 (2012).

19.) S. M. Vinko and 30 co-authors, "**Creation and Diagnosis of a solid-density plasma with an X-ray free-electron laser**", Nature **482**, 59 (2012); R. Nagler, SLAC preprint "**Matter in Extreme Condiion at X-ray free-electron lasers**".

20.) A. Osterheld, J. Dunn, B. Young, S. Libby and A. Szoke, "**Na-like autoionizing levels: plasma diagnostics and prospects for photopumped soft X-ray lasers**", AIP Conference proceedings 332, 215 (1995); S. Libby, A. Osterheld, A. Szoke, R. Walling and B. Young, "**Progress toward X-ray lasing between autoionizing transitions**", UCRL-JC-109842.

2.) Experimental context for MD+CR

In this proposal we demonstrate the feasibility of combining molecular dynamics (MD) particle simulation with atomic kinetics (e.g,. in the collisional-radiative model, hereafter denoted CR). There are many potential applications for this combinatin of existing computational methods. In this section we describe the experimental context for one class of applications. After briefly describing X-ray laser interactions with matter, we mention some other possible applications. The work performed for this project during FY13 was aimed at Japanese X-FEL experiments on iron foil targets.

2A.) XFEL target interactions

The X-ray free-electron laser is something new under the sun. Scientists in California will be most familiar with the LCLS facility recently completed at SLAC (Stanford Linear Accelerator Center) but, in fact, comparable machines are being built in Harima, Japan, in Hamburg, Germany and in Pohang, South Korea.

The machines produce short pulses (10 -100 fs) of multi-keV X-rays, which can be focused to high intensity. An entirely new category of target interaction experiments becomes possible with these x-rays. The machines can also perform conventional X-ray diffraction experiments which will compete for machine time with the new science.

We can cite two dramatic examples,
1.) Justin Wark and collaborators[1] performed a remarkable high-intensity interaction experiment in which aluminum metal targets are "bleached" by removal of inner-shell electrons. X-ray fluorescence is observed from each possible charge state. Analysis of the spectra[2] has given an experimental measure of continuum depression which disagrees with (some of) the conventional wisdom. This experiment was performed at LCLS with 1.5 keV X-rays focused to intensities ~ 10^{17} W/cm^2.

2.) Nina Rohringer, Jim Dunn and collaborators[3] pumped Neon gas with 0.8 keV X-rays and observed inner-shell laser emission, realizing a long-awaited dream of inner-shell X-ray lasers. (Duguay[4], Lan and Meyer-ter-Vehn[5])

Japanese X-FEL Experiments

The Japanese XFEL experiments are performed on an electron linac named SACLA located at the SPring-8 light-source facility in Harima, Japan[6]. SACLA is about ¼ mile long and has undulator(s) generating an X-ray Free Electron laser (XFEL). It is significantly smaller than LCLS because it uses higher-frequency electronics ("C-band"). SACLA produces about ½ millijoule of X-rays per pulse, tunable, with photon energies of 7 -10 keV for the experiments discussed here. The X-ray pulse duration is 10 fsec and the rep-rate is about 20 Hz. These parameters are interesting but not amazing. However, using two-stage Kirkpatrick-Baez focusing optics, *the X-rays are focused to a 50 nanometer focal spot.* The spot-size is confirmed by imaging wire arrays placed upstream from the best focus. The focused energy is probably only one percent of the

SACLA output (~ 20 microjoules), but reaches intensities up to 10^{20} Watts per cm^2 on and inside the target.

Such high intensities were achieved with ultra-short pulse visible lasers ("petawatt lasers") but never before with hard X-rays. The intensity quoted is about 1000 times brighter than the best published result from LCLS, but obviously the LCLS team has plans to improve their focusing optics. Our calculations confirm the claimed high intensities because we find the observed bleaching phenomena do not occur for Fe at lower X-ray intensities.

Focal spot geometry

In the SACLA experiments led by Prof. H. Yoneda of the UEC (Tokyo), Fe foils of 10, 20 micron thickness are irradiated by the X-FEL focused by a long focal-length lens. The x-rays effectively create a thin tube (cylinder) of heated material running through the foil. The focal spot size is about 50 nanometers diameter but the post-shot damage spot is about 1 micron in radius. At lower intensity (up to, say 10^{18} Watt/cm^2) the x-rays are simply absorbed according to the cold-matter absorption coefficient, but above that intensity enough K-shell holes (removed electrons) are produced to significantly reduce the absorption and increase the transmission. This is the *bleaching*.

The Japanese experiments have special features which simplify the requirements for modeling, and our computer code should ultimately be able to handle more general situations. A first special feature is the short X-ray pulse duration. There is not much atomic motion during 10-20 femtoseconds, so the MD part of the calculation is not heavily tested. Second, the SACLA experiments do not yet have high-resolution spectroscopy, so the interesting effects of transient ionization on the line profiles are not yet measured. Our computer calculations can suggest or predict future experiments with better diagnostics. A third special feature is the *one-way energy transfer*: X-ray energy enters the target atoms as K-shell ionization and then cascades to lower energies without many back-transitions. This is a simplification for atomic modeling. We have tried to exploit these simplifying features. It is obviously a good strategy to develop a new computational model in the context of a specific experiment, taking advantage of any simplifying features. Later the code capabilities and its range of application will be extended.

In summary, the SACLA experiments already achieve amazing parameters, putting tens or hundreds of multi-keV photons per atom in very small focal spot.

Prospects for the X-FEL:

Science with X-ray free electron lasers is likely to grow rapidly because there will soon be four competing facilities: LCLS, SACLA, Hamburg, and the PAL machine in Pohang, Korea. Looking farther ahead, Stanford scientists have announced a miniature linac -- "accelerator on a chip" -- using laser-generated electric fields in fused silica chips. The authors explicitly claim that their technology will ultimately make possible X-ray FELs at the ordinary laboratory (or hospital) size-scale[7].

2B.) The X-Ray laser is a Livermore success story

A first Laboratory soft X-ray laser was demonstrated by LLNL scientists in 1984 and in the years since then Livermore scientists have led the world in the development of X-ray laser science. We can gather the history of these Laboratory XRL experiments into three groups:

1.) The first proof-of-principle experiments, a large team effort led by Dennis Matthews and Mordy Rosen[8, 9].

2.) A period of consolidation and application, which demonstrated lasing at shorter wavelengths in various isoelectronic sequences, used short-pulse optical lasers to pump the lasers and demonstrated interferometry, holography and imaging of small specimens, work of J. Trebes, J. Dunn, A. Osterheld, S. Libby and many others.[9-21]

3.) A recent move to use X-rays from the X-FEL for target interaction experiments including pumping inner-shell lasers[1-3, 22-23].

Livermore hosted several workshops to study potential applications of X-ray lasers. In most cases, the applications to biology or other science required:

a.) Shorter wavelengths λ ("water window")
b.) Shorter pulses to beat hydrodynamic expansion of the heated target
c.) High rep-rates to obtains significant amounts of data
d.) Better mode-control for quantum optics

Essentially all these wishes are now granted by the x-ray FEL sources.

These comments and references give a superficial overview of the XRL research performed at LLNL since 1984. During the coming year, we will propose to edit a collection of the main LLNL published research on Laboratory laser-pumped X-ray lasers. This collection would be an invaluable desk-top reference for a new generation of scientists working on XFEL-pumped X-ray lasers.

The new simulation technique of MD + CR is an ideal modeling tool for future X-ray laser experiments because it can combine first-principles calculations of (a.) inversion kinetics, (b.) line-broadening physics, and (c.) line-formation, gain narrowing, etc.

2C.) MD+CR for opacity of dense plasmas

The combination of molecular dynamics with atomic kinetics has a broader range of applications.

Opacity is the X-ray absorption and emission cross-section for hot plasmas and plays a vital role in several branches of pure and applied science. Opacity is a key material property that controls the internal structure of a star because the star must succeed to emit the energy it produces or it will explode. For inertial fusion target experiments, the opacity of target materials is a key material property controlling the

generation of high pressures for the implosions. Existing opacity data may not be sufficiently accurate to support the elaborate fusion experiments performed at NIF[24].

Opacity depends critically on atomic spectra: line profiles, line shifts, edge structure, and continuum lowering. While all these topics can be treated by plasma kinetic theory and have been studied since the 1930's, various uncertainties arise from approximations ("random phase approximation", "local field" corrections, etc) and from possible interactions between multiple processes which occur at the same time in the plasma if not in the theory. That there is still some uncertainty for the opacity of dense plasmas is clearly shown by the results of the Justin Wark LCLS experiment[2].

MD + CR calculations offer a fresh approach to the theory of opacity, based not on complicated theoretical arguments and approximations, but rather on large-scale particle simulations and careful analysis to confirm or challenge the kinetic theory.

A typical application of MD + CR would be to study the effect of collisions on line profiles. In a dense plasma the collisions can be more rapid than the emission of radiation. It is known for a number of years that collisions can change even the simplest line profile (Doppler profiles) in a way that is not encompassed by existing opacity codes[25]. The combination of MD with the collisional-radiative (CR) model cannot address this phenomenon but a similar combination of MD with the density-matrix Schroedinger equation can do so. It seems clear that similar effects of collisions on Stark or other profiles have received insufficient study. The effect of collisions on Doppler and Stark broadening can be studied by MD + quantum atomic kinetics based on the Schroedinger Eq.; we present a feasibility study for this class of calculations in section 8 below.

NLTE opacity raises additional questions about line formation, escape factors and laser gain narrowing. MD+CR calculations of these processes would raise (or lower) our confidence in practical models that are widely used.

A more fundamental scientific application of MD + atomic kinetics would be the important field of trapped atoms, laser cooling and production of "entangled" states. These topics could also be studied by many-atom Schroedinger Eq. calculations, if those calculations are found to be feasible (see section 8 below).

2D.) Particle simulation of reacting plasmas

Inertial fusion ignition simulation

Another context for impoved MD particle simulation is the physical behavior of inertial fusion targets. Currently these are simulated by large radiation-hydrodynamic codes which combine many processes and attempt to follow the entire evolution of a target from its cryogenic starting point at ~ 17 K to the ~ 60,000,000 K burning plasma.

The processes are described by formulas derived by theorists over the past 50 years, but there are clearly imperfect aspects of these formulas because the experiments do not always agree with the computer simulations[24].

Molecular dynamics particle simulation of small regions in a fusion plasma can, in principle, test and/or correct the formulas used in the hydrodynamic codes. The particle simulation has the advantage that it need not assume local equilibrium (Maxwellian velocity distributions). The particle simulation also can treat situations where many types of non-equilibrium occur together. With particle simulation the diagnostics are effectively unlimited.

Fusion ignition particle simulations reported in refs. (26, 27) include D, T ions, ion-ion collisions, electron-ion coupling, fusion reactions, production of energetic alpha particles and neutrons, alpha-particle collisions with ions and energy-loss to electrons, and the absorption and emission of x-rays.

The calculations performed do not include impurities but clearly impurities play a significant role in the experiments. A key requirement for treating impurities in such particle simulations will be the atomic processes - atomic kinetics, radiation coupling and ionization - on the impurity ions. For this reason even the fusion simulations will benefit from the combined MD + CR modeling.

REFERENCES

(1.) S. M. Vinko and 30 co-authors, "**Creation and Diagnosis of a solid-density plasma with an X-ray free-electron laser**", Nature **482**, 59 (2012).

(2.) O. Ciricosta and 31 other co-authors, "**Direct measurement of ionization potential depression in a dense plasma**", Phys. Rev. Lett. **109**, 065002 (2012).

(3.) N. Rohringer, D. Ryan, R. London and nine other co-authors, "**Atomic Inner-shell X-ray laser at 1.46 nanometers pumped by an X-ray free-electron laser**", Nature **481**, 488 (2012).

(4.) M. Duguay, "Soft X-Ray lasers pumped by photoionization", p. 557 in **Laser Induced Fusion and X-ray laser studies**, Ed. by Jacobs, Scully, Sargeant and Cantrell, Addison-Wesley Publishing Co., 1976.

(5.) Ke Lan, E. Fill and J. Meyer-ter-Vehn, "**Photopumping of XUV lasers by XFEL radiation**", Laser and Particle Beams **22**, 261 (2004).

(6.) H. Yoneda and 9 co-authors, "**Nonlinear optics for multi-keV X-ray lasers**", preprint. H. Yoneda et al., unpublished. Dr. Yoneda showed his recent experimental results in a LLNL seminar on August 14, 2013, and we discussed further with him in off-site meetings.

(7.) Peralta et al., Nature, Sept. 2013 (unpublished press-release).

(8.) "**Demonstration of a Soft X-ray Amplifier**", D. Matthews, P. Hagelstein, M. Rosen and 16 other co-authors, Phys. Rev. Lett. **54**, 110 (1985).

(9.) "**Exploding-foil technique for achieving a soft X-ray laser**", M. D. Rosen, P. Hagelstein, D. Matthews and 10 other co-authors, Phys. Rev. Lett. **54**, 106 (1985).

(10.) "**Demonstration of soft x-ray amplification in Ni-like ions**", B. J. MacGowan, S. Maxon and 7 other co-authors, Phys. Rev. Lett. **59**, 2157 (1987).

(11.) "**Theory and design of soft X-ray laser experiments**", R. London, M. Rosen, S. Maxon, D. Eder and P. Hagelstein, J. of Phys. **B22**, 3363 (1989).

(12.) "**Demonstration of X-ray amplification in transient gain Ni-like Palladium scheme**" (sic), J. Dunn, A. Osterheld, R. Shepherd, W. White, V. Shlyaptsev and R. Stewart, Phys. Rev. Lett. **80**, 2825 (1998).

(13.) "**Gain saturation regime for laser driven tabletop Ni-like ion X-ray lasers**", J. Dunn, Y. Li, A. Osterheld, J. Nilsen, J. Hunter and V. Shlyaptsev, Phys. Rev. Lett. **84**, 4834 (2000).

(14.) "**Demonstration of X-ray Holography with an X-ray Laser**", J. Trebes, S. Brown, E. M. Campbell, D. Matthews, D. Nilson, G. Stone and D. Whelan, Science 23 October 1987: 517-519. [DOI:10.1126/science.238.4826.517]

(15.) "**Ultrahigh-Resolution X-ray Tomography**", W. S. Haddad, I. McNulty, J. E. Trebes, E. H. Anderson, R. A. Levesque, and L. Yang, Science 18 November 1994: 1213-1215. [DOI:10.1126/science.266.5188.1213]

(16.) "**Natively Inhibited Trypanosoma brucei Cathepsin B structure determined by using an X-ray laser**", Lars Redecke, Karol Nass, Daniel DePonte and 46 other co-authors, Science **339**, 230 (2013).

(17.) "**Measurement of the Spatial Coherence of a Soft X-Ray Laser**", J. E. Trebes, K. A. Nugent, S. Mrowka, R. A. London, T. W. Barbee, M. R. Carter, J. A. Koch, B. J. MacGowan, D. L. Matthews, L. B. Da Silva, G. F. Stone and M. D. Feit, Physical Review Letters **68**, 588 (1992).

(18.) "**Na-like autoionizing levels: plasma diagnostics and prospects for photopumped soft X-ray lasers**", A. Osterheld, J. Dunn, B. K. F. Young, S. B. Libby, A. Szoke, R. Walling, W. H. Goldstein, R. E. Stewart, A. Faenov, I. Yu. Skobelev and S. Ya. Khakhalin, AIP Conf. Proc. 332, 215 (1995).

(19.) "**Progress toward X-ray lasing between autoionizing transitions**", S. Libby, A. Osterheld, A. Szoke, R. Walling, B.K.F. Young, UCRL-JC-109842 (June 25, 1992).

(20.) "**Wavelength choice for soft x-ray laser holography of biological samples**", R. A. London, M. D. Rosen and J. E. Trebes, Applied Optics **28**, 3397 (1989).

(21.) "**Dynamics of biological molecules irradiated by short x-ray pulses**", S. Hau-Riege, R. A. London, A. Szoke, Physical Review **E 69**, 051906 (2004).

(22.) N. Rohringer, R. Santra, "**Resonant Auger Effect at High X-ray Intensity**", LLNL-JRNL-403123 (April 24, 2008).

(23.) "**Atomic inner-shell x-ray laser pumped by an x-ray free-electron laser**", Nina Rohringer and Richard London, Phys. Rev. **A80**, 013809 (2009).

(24.) U.S. Department of Energy Report to Congress, December 2012, **NNSA Path Forward to Achieving Ignition in the Inertial Confinement Fusion Program**; W. Goldstein, Ed., Report LLNL-TR-570412, Science of Fusion Ignition on NIF, May, 2012.

(25.) D. Burgess, D. Everett and R. Lee, J. Phys **B12**, L755 (1979).

(26.) R. More, "**Particle Simulation Code for Fusion Ignition**", in Nuclear Instruments and Methods A, 2013.05.067 (2013).

(27.) R. More and F. Wang, "**Molecular dynamics with atomic transitions and nuclear reactions**", 24th IUPAP Conference on Computational Physics (IUPAP-CCP 2013), Journal of Physics Conference Series **454**, 012027 (2013).

3.) Molecular Dynamics and Collisonal Radiative Atomic Kinetics

This section will present a brief background of the methods used in the work performed for this project. The narrative will emphasize fundamental questions about the limitations of the methods used.

3A.) **MD/MC** methods were invented in Livermore

Molecular dynamics particle simulation using digital computers was introduced by B. Alder and T. Wainwright in 1957[1]. MD studies a system of particles which can represent atoms, molecules or ions. Each atom has classical coordinates $\mathbf{R}_j(t)$, $\mathbf{V}_j(t)$ and moves according to Newton's laws (= classical mechanics) governed by forces from the neighbor atoms.

For many years the particles were structureless hard disks moving in 2D or hard spheres in 3D or simple point charges and the goal was to study the many-body equation of state or transport properties. Early calculations showed that particles rapidly relax to a Maxwell distribution as a result of binary collisions; this was regarded as an important confirmation of basic ideas of statistical mechanics[2]. Our own modest involvement in this research was a comparison of heat conduction in a rotating disk calculated by molecular dynamics with the result obtained by solving an appropriate Boltzmann equation; the two solutions agreed[3].

In 1966, Brush, Sahlin and Teller[4] applied the complementary technique of Monte Carlo (MC) simulation to the equilibrium statistical mechanics of point charges in dense plasma. H. DeWitt, among others[5,6], extensively studied the properties of strongly coupled (dense) plasmas using Monte Carlo simulations.

Simpler MC methods are widely used for engineering calculations of radiation or particle transport, e.g., for neutron transport in nuclear reactor kinetics, or for stopping of fast charged particles (radiation damage).

A new direction for these methods is particle simulations in which *the particles can change state*. This can occur as a result of internal excitation or as a consequence of chemical or nuclear reactions.

This idea of combining Molecular Dynamics with Atomic Kinetics (MD + CR) has motivated several research groups. A Livermore group led by F. Graziani and J. Glosli works from an existing particle simulation code (ddcMD code)[7]. This author worked with their group during 2005-2010, learning computational techniques and making an independent assessment of priorities[8,9]. The Graziani team has analyzed experiments that use X-rays from LCLS as *diagnostics* of plasmas heated to WDM temperatures by a short-pulse optical laser[10]. For the most part, they decided to develop MD simulations in which the electrons are treated as classical particles and use pseudopotentials to try to improve the low-temperature electron correlation behavior. This author has explored a different path, treating the electrons as a fluid (as in the usual plasma CR model) and looking at high temperatures where electron correlations are generally less important. Treating the electrons as a fluid has the practical advantage of making possible much larger computational time-steps, and this made it possible to

perform 10 psec simulations of DT plasma ignition at conditions similar to NIF experiments.[1,3]

G. Faussurier and C. Blancard, at the CEA Laboratory in Bruyeres-le-Chatel, are working to develop a CR+MD simulation code. They have discussed the difficulty of reconciling the treatments of bound and free electrons when the electrons are treated as classical particles.

MD + CR particle simulation methods are sharply distinct from the well-known and well-developed method of *Quantum Molecular Dynamics* (QMD) which describes equilibrium (LTE) conditions, usually at relatively low temperatures. The QMD method combines particle ions with a (quantum) density-functional treatment of electrons. The simulations generally are followed long enough for the ions to reach equilibrium. The MD + CR technique is more appropriate to violently non-equilibrium plasmas in which the atomic states and/or ion velocities do not have equilibrium (Maxwell-Boltzmann) distributions. MD + CR would simulate the time-evolution.

In MD particle simulations, the atomic motion is controlled by forces between atoms. For X-ray FEL targets starting at room temperature, the atomic forces begin as the usual chemical bond forces. As the target heats, the forces change to screened-Coulomb repulsions between ions. The numerical techniques (differencing of the equations of motion) are straightforward for atomic motion. The interesting new questions are *managerial:* how to find which atoms or ions are close to a given one, when to update lists of particles, and how to implement reactions or transitions which change the properties of the particles.

We simulate a small volume embedded in a surrounding homogeneous plasma using periodic boundary conditions. It was shown by Kohn and Butler[14] that simulation of a random system using periodic boundary conditions converges exponentially to the infinite-system limit, i.e., converges more rapidly than any other boundary condition.

For our calculations, we must exercise judgement about how to treat particles that have long mean free paths. Multi-keV Auger electrons or fluorescent X-rays generally escape from the X-FEL interaction region, typically a 50 nm diameter tube under the focal spot. (The question whether this interaction region becomes highly charged is discussed below and in Appendix D; our conclusion is that for metallic targets it probably does not.)

For iron foil irradiation by the X-FEL, we begin the calculation with a large number $N_{at} \sim 20{,}000$ of neutral Fe atoms in the bcc lattice of room-temperature α-Fe. The atoms interact by a short-range Morse potential U(r) whose parameters (range, well-depth, small-r stiffness parameter) are not optimized but are consistent with the correct solid density and an approximately correct sound-speed.

The simulation cell uses periodic boundary conditions. Atoms are located using a sub-box structure: the simulation cell is divided into $11^3 = 1331$ sub-boxes matched to the bcc lattice (each sub-box contains 8 unit cells). Atomic forces are re-calculated on each MD time-step from the ~ 430 atoms in 27 sub-boxes surrounding a given atom. Each computational sub-box begins with 16 atoms, but the atoms are free to move across the sub-box boundaries. With rising temperature and increasing ionization, the forces

change to screened Coulomb potentials. Atoms leave their lattice positions and move under their interatomic forces, but do not move large distances in 10-20 fsec. Even with a relatively large time-step for the ion motion, the MD part of the calculation, especially the pair-force calculation, requires most of the computer time. Results from the MD+CR simulation are shown in section 9 below.

The code uses a system of pointers which identify which sub-box a given ion occupies and maintain a (constantly changing) list of which ions occupy each sub-box. Combining the pointers and lists, we can rapidly locate the neighbors of any given ion. The force-laws change as ionization occurs during the calculation and these changes should be consistent with changes of the ionization potentials (i.e., with the atomic processes). This consistency it is not yet enforced in our codes, but would be needed to obtain energy conservation at the "eV" size scale. At present the code conserves energies on the "keV" scale. When the forces and atomic energies are consistent the code will be better able to predict line profiles.

3B.) Atomic Kinetics and the CR model

Usual CR model

The Collisional-Radiative model (CR model) for atomic kinetics was developed to analyze experimental spectra from astrophysics and from laboratory experiments on magnetic fusion. British scientists (Bates, Kingston and McWhirter, Seaton and others) took an early lead, based on their strength in atomic data. In the 1980's LLNL assembled strong research teams and developed powerful CR computer codes for various applications, especially X-ray laser research.

In some cases the CR codes were integrated with radiation-hydrodynamic simulation codes and in other cases they were stand-alone code packages. Well-known examples are the YODA code of P. Hagelstein or the CRETIN code written by H. Scott[15]. Theory of CR models is reviewed in textbooks by Griem[16], Salzmann[17] and Fujimoto[18].

The Collisional-Radiative (CR) equations can be schematically written

$$\frac{\partial N_j}{\partial t} = \sum_{j'} T_{j,j'} N_{j'} - N_j \sum_{j'} T_{j',j} \qquad (3\text{-}1)$$

$T_{j'j}$ is the transition rate matrix-element for collisional and radiative transitions j --> j'. The symbol j represents both ionization and excitation state. Again schematically,

$$T_{j',j} = n_e \langle \sigma_{j \to j'} v \rangle + A_{j \to j'} (n_\nu + 1) \qquad (3\text{-}2)$$

The first term $n_e < \sigma v >$ denotes electron collisional transitions from j to j' and the second term A (n_ν + 1) denotes spontaneous and stimulated emission of radiation. There can be

many other processes; for example Auger transitions (autoionization) or dielectronic recombination. Some formal mathematical properties of the CR kinetic equations are summarized in reference 19. For inner-shell Auger and emission processes which are most important for X-FEL target interaction, it is convenient that although the rates are very different for different excitation/ionization states, they do not depend strongly on plasma ρ, T conditions.

Although CR models have been thoroughly explored for many decades, there remain important uncertainties. In a finite geometry, so-called *escape factors* are introduced to represent the fraction of emitted photons that leave the plasma through a distant surface[20]. These factors are obtained from statistical calculations for idealized models and are a source of uncertainty in any specific application. The MD+CR metod, when implemented on large computers, can provide reliable numerical calculation of escape factors.

In section (3e) below we discuss another weak point of the CR model.

3C.) Performance figures of merit

Molecular Dynamics (MD) calculations can be performed with many millions of particles (large N_{atoms}) and using such large numbers appears to be a point of pride for users of large supercomputers. Simulations with large numbers of particles can be expected to have smaller numerical fluctuations.

For MD calculations, the choice of interatomic pair potentials seems to be the main physics question. For our purpose, reactions can change the particles during the calculation. These changes imply abrupt changes in the pair potentials and those changes have implications for energy conservation. Thus energy conservation and the number of particles are the usual performance measures for MD calculations.

Collisional-radiative calculations with many thousands of excited states are not unusual. Probably the main difficulty for a collisional radiative model with N_{lev} excited levels is that all the N_{lev}^2 rates should be correct. An important point: the CR model gives no warning if an important process has been left out or if the rates are incorrect. The best available test is to compare to experimental spectra.

3D.) Practical considerations

A simple combined MD + CR calculation would try to evolve $N_{atoms} \times N_{levels}$ variables. With 20,000 atoms and 100 levels, this is 2 million variables, within the reach of modern desk-top computers. However it is possible to be more efficient.

The MD+CR calculation will describe effects of atomic motion (Doppler shifts and changes of collision rates caused by ion motion) and also effects of the time-dependent local environment around each atom. For example, in the MD each atom has

different numbers of neighbor atoms in different charge states. The usual CR model averages these local inhomogeneities.

Treatment of the electrons

A key practical question is how to handle the free electrons. Treating the electrons as particles encounters several difficulties: Recombination into quantized bound-states is difficult for classical particle electrons; classical motion of particle electrons inside atoms is a problem, both for the physics and for the numerical methods. Several research groups have discussed the difficulties of this approach[7, 8, 9, 10, 11, 12].

For example, if one attempts to develop a classical "pseudopotential" which imitates the quantized motion of electrons inside a many-electron ion, this will be so different from the Coulomb potential that it is unlikely to give accurate results for impact ionization, radiation absorption/emission and Auger processes. The quantization of electron motion is not a consequence of some strange potential, rather it comes from the Schroedinger equation.

Our own experience of MD simulations with classical point-charge electrons moving among ions found satisfactory energy conservation only with a very small time-step $\sim 10^{-21}$ sec (this was for low-Z plasmas with keV temperatures). For an electron moving inside a hydrogen atom, the orbit time for the 1s-state is $\sim 8.6\ 10^{-17}$ sec; for Fe K-shell electrons this would be $\sim 2.7\ 10^{-20}$ sec. The simulation time-step dt must be 20 or 30 times smaller to accurately resolve the motion.

3E.) Electron fluid and Markov CR

For this work we adopted two strategies. These are evidently sufficient to successfully combine MD with CR. Although these methods give good results we think it will be important to continue to explore other methods of calculation because there are many possible methods and some may be better adapted to very large supercomputers.

1.) Electron fluid

We treat the free electrons as a "fluid" (just as in the CR equations written above) rather than as classical particles. This one step already makes a big improvement in the simulation time step (factor > 100). It is not necessary to assume the free electrons have a Maxwellian distribution, but that assumption is easy and not too inappropriate for WDM conditions.

For fusion simulations, we needed an efficient treatment of electron-ion coupling, which is important for stopping of fast alpha particles and for transfer of heat from electrons to the DT ions. For that purpose we used Langevin electron-ion coupling formulas based on the work of Chandrasekhar[11, 21]. This method reproduces well-known results for electron-ion energy-exchange and dE/dx to electrons.

2.) **Markov CR method**

Reference (21) proposes a "Markov" version of the CR model. This Markov method looks different from Eqs. (1-2) above, but is probably entirely equivalent in the limit of large numbers of copies of the system. The Markov method has special advantages for physics and for computational implementation in an MD simulation.

In the Markov method, each atom is taken to be in a definite quantum state j during each time-step. The transitions are "quantum jumps" j --> j' governed by probabilities

$$P_{j-->j'} = dt\, T_{j',j} \qquad (3\text{-}3)$$

where dt is the time-step used for the atomic model and $T_{j',j}$ is the transition rate for transitions j --> j'. Typical inner-shell rates are 10^{12} to 10^{15}/sec. When the time-step dt is $\sim 10^{-17}$ sec, the probabilities can be normalized to unity and in fact "no transition" is most likely. Monte Carlo tests to decide which transition occurs can be organized to consider this most-likely case first and doing so speeds the code significantly. This Markov method was proposed for use with MD and tested in reference (21), where it was shown to agree closely with solutions of the usual CR equations.

Since the Markov method looks different from the usual CR equations we made additional tests to verify that the two methods get the same answers. For the tests both calculations use the same initial conditions and the same time step dt $\sim 10^{-17}$ sec. The agreement is excellent. Figure (5-1, 5-2) shows a comparison for time-dependent inner-shell populations of Fe under X-FEL irradiation. The points (Markov) fall on or close to the curves (CR) except for states with very small populations.

Comparison of usual CR with the Markov method:

1.) The usual CR method requires storing populations N_j for all states of all the ions. We use 48 states in the calculations shown in Figs. (5-1, 5-2), and there is an "old" and "new" version of each population: this requires about 100 floating-point numbers per ion. The Markov method only requires storage of one integer (the current state) for each ion, so it has a substantial advantage (factor $\sim$ 100) for large calculations.

2.) Populations from the Markov method fluctuate, and the results depend on the number of ions. Because $(20{,}000)^{1/2} \sim 141$, we expect fluctuations of ~ 0.7 %. Fluctuations are visible in Fig. (5-1, 5-2) but actually the two methods agree surprisingly well even for states with small populations.

3.) The Markov method has another advantage in combination with the MD. In the Markov method, each ion is in a definite charge state during each time-step. This means we can use the current ion charge in the ion pair-interaction forces. The usual CR method does not have a unique charge state.

CR and Quantum Mechanics

Probably most users of the CR method consider it to be a straightforward application of quantum mechanics. One can use accurate energy-levels E_j for the excited states and the cross-sections or radiative rates can be calculated by separate quantum calculations. At low densities, these are certainly good approximations but at high densities the perturbations from the local atomic environment are so frequent and so strong that quantum processes (like collisional excitation or emission of radiation) are no longer purely binary interactions.

For example, radiative lifetimes range from femtosecond (for Fe core levels) to μsec (for hydrogen). Such slow processes can be interrupted by other processes. For Fe K-shell holes, the Auger and radiative rates are approximately equal and it is not obviously justified to simply add these as independent parallel processes.

The Markov CR method dramatically displays this question. The assumption that each atom is in a definite quantum state at each instant, and then abruptly changes state with transitions, is equivalent to assuming there are constant measurements of the state of the system. The errors from such measurement are widely discussed as "Quantum Zeno" effects.

A correct quantum time-evolution would write the state of an atom as

$$\Psi(t) = \sum_j a_j(t)\ \psi_j \qquad (3\text{-}4)$$

and would evolve the expansion coefficients $a_j(t)$ by the time-dependent Schroedinger equation. Instead, the CR model forms

$$N_j(t) = | a_j(t) |^2 \qquad (3\text{-}5)$$

and evolves $N_j(t)$ by Eqs. (3-1, 2). Clearly the CR method of calculation omits a variety of interference effects.

One example of the omitted effects is shown by considering the Stark effect when the atom is in the time-dependent electric field of neighbor ions. The normal CR method simply attaches a separately calculated Stark profile reflecting the average ion in an average plasma whereas the quantum calculation described above (and in section 8 below) would find the response to the instantaneous electric fields by solution of the Schroedinger equation.

Both methods -- Markov sampling and the original CR rate equations -- are equivalent to "repeated measurement" on each time-step, and project a quantum superposition of excited states into a definite excitation state. This approximation is accepted without comment for most plasma spectroscopy research. It is clear that it is incorrect in principle, but not clear how large are the corrections. In the future we will test this approximation by numerical solutions of the atomic Schroedinger equation.

3F.) Questions:

As we develope the atomic kinetics part of this project, we have the following questions:

1.) What processes must we include? What are their uncertainties? (section 4)

2.) Is Markov CR = normal CR ?? (section 5)

3.) Is there an effect of the constant measurements:

$$a_j \Longrightarrow N_j = |a_j|^2$$

The Markov CR method makes this assumption sharp and clear but in truth the same approximation is used in all CR work. "Quantum Zeno" effects may or may not be very large, but quantum mechanics is different from classical mechanics and the quantum theory is correct. (section 8)

4.) MD versus macroscopic modeling

The SACLA XFEL focal spot is long (20 micron) and thin (50 nm) How many heated atoms are there? Is the focal spot highly charged? Do energetic Auger electrons escape? Does emitted radiation escape? (Appendix D)

This question is especially important because it decides whether we need to include electron collisional excitation in the CR model. If the Auger electrons escape, the ambient plasma has a temperature < 100 eV and electrons from that plasma probably cannot significantly excite inner-shell core levels of the Fe ions.

REFERENCES

(1.) B. Alder and T. Wainwright, J. Chem. Phys. **27**, 1208 (1957); J. Chem. Phys. **31**, 459 (1959).

(2.) C. Kittel, **Elementary Statistical Mechanics**, J. Wiley and Sons, 1958.

(3.) W.G. Hoover, B. Moran, R. More and A. Ladd, Phys. Rev. **A 24**, 2109 (1981).

(4.) S. Brush, H. Sahlin and E. Teller, J. Chem. Phys. **45**, 2102 (1966).

(5.) D. Frenkel and B. Smit, **Molecular Simulation**, Academic Press, San Diego, 2002.

(6.) J. P. Hansen, Phys. Rev. **A8**, 3096 (1973); J. P. Hansen and I. R. MacDonald, **Theory of Simple Liquids**, Academic Press, London (1976).

(7.) J. Glosli, F. Graziani, R. More, M. Murillo, F. Streitz and M. Surh, J. Phys. **A 42**, 214030 (2009).

(8.) R. More, F. Graziani, J. Glosli and M. Surh, High Energy Density Physics **6**, 29 (2010).

(9.) R. More, M. Goto, F. Graziani, P. Ni and H. Yoneda, Plasma and Fusion Research **5**, S2008 (2010).

(10.) S. P. Hau-Riege, J. Weisheit, J. Castor, R. London, H. Scott and D. Richards, "Modeling quantum processes in classical molecular dynamics simulations of dense plasmas", New Journal of Physics **15**, 015011 (2013).

(11.) R. More, "Particle Simulation Code for Fusion Ignition", in Nuclear Instruments and Methods A, 2013.05.067 (2013).

(12.) G. Faussurier and C. Blancard, personal communication.

(13.) A. Mattsson, P. Schultz, M. P. Desjarlais, T. Mattsson and K. Leung, "Designing meaningful density functional theory calculations in materials science -- a primer", in Modeling Simulations in Material Science and Engineering **13**, R1 (2005).

(14.) W. Butler and W. Kohn, "Local Theory of Disordered Systems", p 465 in Electronic Density of States, NBS special publication **323**, L. H. Bennett, Ed., U.S. Government Printing Office, 1971.

15.) H. Scott, "CRETIN", JQSRT **71**, 689 (2001).

16.) H. R. Griem, **Principles of Plasma Spectroscopy**, Cambridge University Press, Cambridge, 1997;

17.) D. Salzmann, **Atomic Physics in Hot Plasmas**, Oxford, 1998.

18.) T. Fujimoto, **Plasma Spectroscopy**, Clarendon Press, Oxford, 2004.

19.) R. More, T. Kato, S. Libby and G. Faussurier, JQSRT **71**, 505 (2001).

20.) D. Eder, H. Scott, S. Maxon and R. London, Applied Optics **31**, 4962 (1992).

21.) R. More and F. Wang, "**Molecular dynamics with atomic transitions and nuclear reactions**", 24th IUPAP Conference on Computational Physics (IUPAP-CCP 2013), Journal of Physics Conference Series **454**, 012027 (2013).

4.) Atomic states and atomic rates

In this report we describe an effort to model the SACLA X-FEL experiment on Fe foil targets, and so our chief interest is in Fe inner-shell excited states and process rates. For this purpose we cannot use standard modeling codes: for example, autoionization (the Auger effect) plays an essential role in the X-FEL experiments but is not even included in the inline atomic model used by most radiation-hydrodynamic codes because it is a two-electron process.

For X-FEL - target interaction, the most important atomic processes appear to be (1.) K-shell absorption of the 7.1 keV FEL X-rays, (2.) autoionization of the resulting inner-shell hole states, (3.) X-ray emission (fluorescence radiation), especially K_α emission, and (4.) recombination of free electrons. Additional processes are discussed below.

The work of assembling the atomic data used in this project was strongly aided by Dr. Feilu Wang of the Beijing Astronomical Observatory who visited U. C. Berkeley Physics Department during June-July-August, 2013. Dr. Wang had already contributed to our previous effort to combine collisional-radiative atomic models with molecular dynamics[1]. Dr. Wang ran the FAC code[2] to produce the atomic energies and rates described here and contributed to the analysis reported in this document.

4A.) Inner-shell excited states

7.1 keV X-ray FEL radiation is mainly absorbed by inner-shell electrons of Fe target atoms. The X-rays are tuned to the Fe K-edge. The cross-section for absorption by a K-shell (1s state) electron is more than ten times larger than the corresponding cross-section for an L-shell electron. Absorption excites a K-shell electron, leaving a "hole". After absorption, various processes (autoionization and emission of fluorescence x-rays) refill the K-shell hole and leave holes in states with higher quantum numbers and eventually the holes can be refilled from the free-electron conduction band of Fe.

The spectrum of the neutral Fe atom is complicated by the open 3d shell, and our atomic data sources give very much detail about many states with small splittings. Early in the project we decided to simplify the level-scheme to keep only n, l quantum numbers rather than the relativistic n,l,j quantum numbers displayed in FAC (Flexible Atomic Code) data. This required summing and averaging over the extra quantum number(s).

In our current data-set, the following inner-shell hole states are included:

Neutral Fe groundstate, denoted GS
One-hole states = {1s, 2s, 2p, 3s, 3p, 3d}
Two-hole states = {1s2s, 1s2p, $2s^2$, 2s2p, $2p^2$, 2s3s, 2s3p, 2s3d, 2p3s, 2p3p, 2p3d, $3s^2$, 3s3p, 3s3d, $3p^2$, 3p3d, $3d^2$}
Three-hole states = {2s2p3p, 2s2p3d, $2p^23d$, $2s3s^2$, 2s3s3p, $2s3p^2$, 2s3s3d, $2p3s^2$, 2s3p3d, 2p3s3p, $2p3d^2$, $2p3p^2$, 2p3s3d, 2p3p3d, $2p3d^2$, $3s^23p$, $3s3p^2$, $3s^23d$, $3p^3$, 3s3p3d, $3p^23d$, $3s3d^3$, $3p3d^2$, $3d^3$}

Barring possible typographical errors, that should be 48 states including the groundstate. Since neutral Fe (= GS) has holes in the 3d shell, when "3d" or "$3d^2$" is written above it means *additional* holes relative to the groundstate.

As mentioned, we decided to simplify n,l,j levels (FAC) to n,l by adding and averaging rates. However the most recent SACLA experiment on Cu targets shows clear resolution of two "K-alpha" lines, produced by transitions 1s --> $2p_{1/2}$ and 1s --> $2p_{3/2}$. To model those experiments, we will prepare a Cu data-set which at least distinguishes the two 2p states.

4B.) Atomic process rates

Absorption from the XFEL

So-called "pump" X-rays ($\hbar\omega$ = 7.1 keV) from the SACLA free-electron laser are absorbed by photoelectric transitions of K-shell and L-shell electrons of neutral Fe. For ions with 1s, 2s or 2p shell holes the absorption edge moves to higher energies and these ions can only absorb by electrons of their L-shell. When there is L-shell absorption, the resulting free electron has high kinetic energy and probably escapes the focal spot (the stopping length for a 10 keV electron is about one micron).

There is some uncertainty about absorption from K-shell by ions with n = 3 holes. The FAC data puts these transitions outside the bandwidth of the XFEL pump radiation, but neither the theoretical energy for the absorption edge nor the experimental bandwidth is perfectly certain.

X-ray emission (fluorescence)

Inner-shell holes can be refilled by emission of soft X-rays. These transitions have rates which range from slow (10^{12}/sec) to fast (~ 10^{15}/sec); the emission occurs in competition with autoionization.

For our purposes the 1s --> 2p transition (which produces K-alpha emission) is especially important. The A-value (spontaneous emission rate) given by FAC for this transition is 0.543 10^{15}/sec.

Auger effect (= autoionization).

For Fe K-shell holes, autoionization is about as rapid as radiation. The Auger transitions, for example (2p --> 1s with 2s --> free), leave the atom with two L-shell holes. The emitted free electron has substantial kinetic energy.

The atomic data that we use comes almost entirely from the FAC (Flexible Atomic Code) written by Ming Feng Gu[2]. Various atomic data specialists assure us that this is a satisfactory data source when the code is run correctly.

For radiative rates, we summed over final states, averaged over initial states in the usual way to project the many possible transitions into the simplified n,l scheme that we are using. We also tested the rates as described in Appendix A.

For autoionization rates, we took the largest rate when there were a variety of subshell rates. The argument for this is that free-electron collisions can rapidly induce subshell transitions so an atom does not stay "trapped" in a state with low autoionization rate but instead rapidly finds the subshell state with the high rate.

Free-electron induced transitions are less important because during most of the X-ray laser pulse the free electrons do not have enough energy to excite inner-shell 2s and 2p hole states. Free-electron collisions can induce subshell transitions (e.g., $2p_{1/2}$ <---> $2p_{3/2}$) and in our calculations it is assumed that these populations are proportional to their statistical weights. The outer electrons (3d, 4s) effectively form the "free electron" conduction band in metallic iron, so the complicated multiplet structure of the partially-filled 3d shell in the isolated-atom is not likely to have experimental consequences in an XFEL experiment on solid-density iron. For other applications or other experimental conditions the electron-impact collisions would be very important.

Recombination

Another important process is recombination of free electrons into holes in the 3d shell. This is 3-body recombination and the recombination energy goes to heat the free electrons. The process is rapid because the energy transfers are not large (~ 20 eV).

Atomic calculations (e.g., FAC code) of the recombination rate are not especially reliable because the free electron states in solid-density Fe are nothing like the 3d-4s states of the free atom. In our atomic model we assume the rate is larger for high-charge ions (Fe^{2+}, Fe^{3+}) on the plausible argument that, due to Mott-Debye screening, the free-electron density near these ions is higher than around neutrals or Fe^{+}.

Even if this recombination rate is very large, we think the "rate-limiting" processes are the Auger and radiative transition that refill deep core holes. If this is correct, the calculation is relatively insensitive to the recombination rate. Further study can clarify this; measurements of the emission spectra for soft photons may enable us to obtain an experimental determination of this recombination rate.

4C.) Testing the atomic data

We tested the process ratios to be sure we understand and believe the FAC data. In Appendix A we describe tests of the radiative rates. We could test the A-values against scaled hydrogenic formulas and by checking they obeyed the usual dipole selection rules. For transitions involving multiple core-holes, there was one active hole (electron) and others which were spectators. For example, the transition $2s^2$ --> 2s2p could be compared to the simpler transition 2s --> 2p. The A-values did not agree (and should not) but when appropriate scaling was applied -- for the number of electrons which can emit and for the overall ω^3 scaling of the radiative rates -- the two rates agreed

to a few percent. Examples are given in Appendix A. These tests verify that the FAC code produces reasonable radiative rates and gives us a basis for predicting transitions involving other states.

The Auger (autoionization) rates are in the expected range. We have a large database of autoionization rates generated by U. Safranova and this gave us a set of comparison numbers. Autoionization rates are approximately independent of atomic number except for obvious constraints on the filling of levels.

4D.) Uncertainties in the atomic kinetics:

It can be useful to list the main uncertainties in the atomic kinetics that we perceive at this writing:

1.) Recombination from free electrons to 3d hole states.

This rate is uncertain because the target interaction involves solid-density Fe, not the free atoms treated by the atomic code. In solid Fe, the 3d-states occupy a band of energies and partially overlap with (and hybridize with) the 4s conduction band per se. That means that a 4s electron can enter a 3d state with no change of energy. Because the free-electrons have temperatures up to 100 eV, the various 3d subshells are probably very rapidly equilibrated.

The XFEL experiments could in principle provide information about this recombination rate if soft x-ray spectra can be obtained. Such data would be of considerable fundamental scientific interest because it bears on the magnetic structure of transition metals, one of the few aspects of solid-state electronic structure not entirely clarified by QMD calculations.

2.) Line shifts and changes of atomic pair-potential

The atomic motion is governed by atomic pair potentials that depend on the state of ionization or excitation of the Fe ions. At the same time, these pair potentials change the ionization potentials (or autoionization energies) of the inner-shell atomic states. The changes are likely to be of the order of 5 or 10 eV and do not affect the calculations reported here, which aim at the keV energies of the core levels. Precise measurements of X-ray fluorescence widths or of the K-alpha line width will provide information necessary to test and verify these important interaction effects. The LCLS experiment of Justin Wark et al.[3] shows an example of this type of analysis.

3.) Subshell redistribution

We have assumed subshell redistribution (e.g., $3p_{3/2}$ <---> $3p_{1/2}$) is rapid but this assumption could be tested by more detailed calculations.

4.) Electron impact by Auger electrons

We assume that Auger electrons are able to leave the focal spot without interacting with the target plasma because it is only 250 Angstroms in radius. Auger electrons have enough energy to ionize or excite Fe atoms and might have consequences that are not included in the calculations reported here.

5.) Escape of emitted photons

We also ignore the possible absorption of the emitted fluorescence radiation in the focal spot region, again on the argument that the SACLA focal spot (tube) is so thin that it cannot be imagined to be optically thick. It would be easy to improve the atomic model to include the absorption of fluorescence radiation and with that improvement, detailed balance could be used as a check. If the code is applied to other experiments in different geometries the absorption could make an important contribution.

6.) Behavior of a non-metallic target

Finally we draw attention to the electrostatic issue: if the target is essentially fully ionized in a 50 nm tube through the foil and if the Auger electrons escape freely, there is the possibility of a high electrostatic potential. In Appendix D we argue that for Fe or other metallic targets, this potential is neutralized very rapidly, but for targets made of insulators (including Fe oxide) the neutralization can only occur by a powerful electrical discharge. Without attempting to analyze that physics, we can see that it would be interesting.

Atomic Kinetics - summary comments

The energies of the core-hole states control the ability of the Fe atom to absorb laser X-rays and the output energies of Auger electrons control the target heating. While the SACLA group has not yet measured soft X-ray emission, we consider it important to predict this potentially valuable diagnostic. Emission of soft X-rays also has a strong influence on target energy balance.

Free-electron induced transitions are less important because during most of the X-FEL heat pulse the free electrons do not have enough energy to excite inner-shell 2s and 2p hole states. Free-electron collisions can induce subshell transitions (e.g., $2p_{1/2}$ <---> $2p_{3/2}$) and in our calculations it is assumed that the subshell populations are proportional to their statistical weights. The outer electrons (3d, 4s) effectively form the "free electron" conduction band in metallic iron, so the complicated multiplet structure of the partially-filled 3d shell in the isolated-atom is not likely to have experimental consequences in an XFEL experiment on solid-density iron. For other applications or other experimental conditions the electron-impact collisions would be very important.

REFERENCES

1.) R. More and F. Wang, "**Molecular dynamics with atomic transitions and nuclear reactions**", 24th IUPAP Conference on Computational Physics (IUPAP-CCP 2013), Journal of Physics Conference Series **454**, 012027 (2013).

2.) Flexible Atomic Code, by Ming Feng Gu, Can. J. Phys. **86**, 675 (2008).

3.) O. Ciricosta and 31 other co-authors, "**Direct measurement of ionization potential depression in a dense plasma**", Phys. Rev. Lett. **109**, 065002 (2012).

5.) Bleaching and gain

The SACLA X-FEL experiments have now observed both bleaching and stimulated emission (gain) from foil targets irradiated by high-intensity x-rays. This section will describe the physics of bleaching and gain in X-FEL interaction with Fe foils. Details of our calculations are given in sections 4, 6 and 9.

5A.) Comparison of Markov CR with the usual CR

Our first concern was to verify that the Markov collisional-radiative calculations agree with the usual CR method. Because the calculations illustrate nicely the atomic physics that underlies the bleaching and gain phenomena, it is appropriate to present them in this section.

It is probably a rigorous mathematical theorem that the Markov CR is exactly equivalent to the usual CR equations *in the limit of large numbers of atoms(ions).* Here we are not concerned with the mathematical limit but rather with the practical question: is it feasible to use enough particles on a desk-top computer so that the Markov and usual CR are essentially the same for the important populations?

To make a fair comparison, the two methods will use the same set of excited states, the same transition rates and the same numerical time-step. For the Markov CR, we did calculations with 20,000 Fe atoms and up to 800,000 atoms. (There was no trouble using such a number of Fe atoms.) Everything reported here was done with the 48-level atomic model described in section 4 and Appendix A.

The X-ray pulse is a 10 fsec (FWHM) Gaussian pulse with a specified peak intensity. The pulse is started when the X-ray intensity is about 1 % of the peak and the peak intensity occurs at about 13 fsec.

The calculations show "local" bleaching in a small volume ~ $(0.02 \text{ micron})^3$. Figure 5-1 shows that at a peak pulse intensity of $5\ 10^{18}$ W/cm^2, the population of the neutral groundstate "GS" falls to ~ 0.5 and consequently the K-shell absorption from this state is reduced by 50%. That means that 50% bleaching occurs in every part of the target where the intensity exceeds $5\ 10^{18}$ W/cm^2 (according to the code model).

The ground-state (GS), 1s and 2p-hole populations are shown in Figures 5-1, 5-2. For these figures the Markov calculations are shown as points and the usual CR rate equations as curves. The agreement is not perfect but entirely satisfactory.

These figures show the atomic physics mechanism for the bleaching phenomenon. The X-ray flux removes K-shell electrons from neutral Fe atoms leaving one K-shell hole per atom. The second K-shell electron cannot be removed in this way because it has a significantly higher ionization potential. However the Auger effect refills the K-shell hole within ~ one fsec. How does the Fe atom remain "bleached"?

Detailed calculations of energy levels with the FAC code (performed by F. Wang) show that if there are one or two holes in the L-shell, the K-shell absorption edge moves to higher energies. Because the SACLA X-FEL pulse has a narrow bandwidth around the K-edge it cannot ionize these excited states. Ionization from the L-shell is always possible but that process has a much smaller cross-section. For the SACLA experiments the X-FEL pulse has a bandwidth of approximately 7.100 to 7.130 keV. This is

sufficiently narrow to assure that Fe atoms with holes in 1s, 2s, 2p states (or 2 holes in the L-shell) cannot absorb with the large K-shell cross-section.

There is a question for the modeling which depends more delicately on the X-FEL bandwidth. This is the question whether Fe ions with one or more holes in the M-shell can absorb. Those holes also shift the absorption edge, but by smaller amounts. For the calculations shown here we assume the X-FEL bandwidth is sufficiently narrow to exclude that absorption but this assumption needs further invesigation. From a computational point of view including the additional absorption would pose no difficulty.

5B.) Calculations of Bleaching

Next we examine the results for bleaching of a foil (i.e., X-FEL transmission through the entire foil). Figures 5-3, 5-4 show calculations from the ray-trace code described in section 6 for transmission of 10 fsec (FWHM) pulses through 10 and 20 micron foils of Fe. The quantity plotted is the ratio of transmitted energy density (J/cm^2) to incident energy density, i.e., the x-ray intensity (W/cm^2) is integrated over the pulse duration.

The bleaching predicted by the calculations occurs at a few times 10^{19} W/cm^2. (That is the peak intensity of the Gaussian pulse.) This calculation is in good agreement with the (unpublished) measurements at SACLA. The agreement is a non-trivial test of our modeling.

We emphasize a key fact for this modeling: with a narrow-band X-FEL pump pulse, the Fe atom cannot absorb via K-shell ionization when there are holes in the 1s, 2s or 2p states (it can still absorb by the smaller L-shell cross-section). In our calculations it is also unable to absorb when there are one or more M-shell holes and that assumption may need to be revisited. In any case, the bleaching persists much longer than the short lifetime (~ 1 fsec) of the 1s hole state.

The intensity for bleaching to occur depends on the target thickness because high transmission requires that the target be bleached all the way through, front to back. The difficult part is the rear surface because the intensity that penetrates to that surface is significantly lower than the incident front-surface intensity.

5C.) Gain for Kalpha radiation

Next we describe calculations of gain on the Kalpha transition (1s --> 2p) for Fe foils. Apparently gain on K_α was observed for Cu (rather than Fe) foils but except for a shift to higher photon energies the physics should be generally very similar.

Our gain calculations use populations from the raytrace code (based on the "usual" CR model) and Eqs. (6-2, 6-3) for the gain. This is a "travelling wave" gain calculation.

Figure (5-5) shows one representative case. With a gL product of ~ 25 for a 10 micron foil, it is clear the local gain is very large.

In Fig. (5-5) the gain across the entire foil is plotted as a function of the start time t_o at which a hypothetical seed pulse enters the front surface. In reality the seed pulse has a finite duration and would propagate as a convolution integral of this instantaneous gain. The important conclusion we draw from Fig. (5-5) is that the gain is large and positive in the first part of the heat pulse (X-FEL pulse) and falls to absorption in the second half of the pulse. The reason for this should be clear from the population time-history shown in Figs. (5-1, 5-2) The early-time inversion disappears as time progresses.

We repeated these calculations for foils of 20 micron thickness, and find the gL integral is accurately linear in the foil thickness L. In an experiment because the amplified seed beam is already entirely saturated we do not expect any significant difference in behavior between the 10 and 20 micron foils.

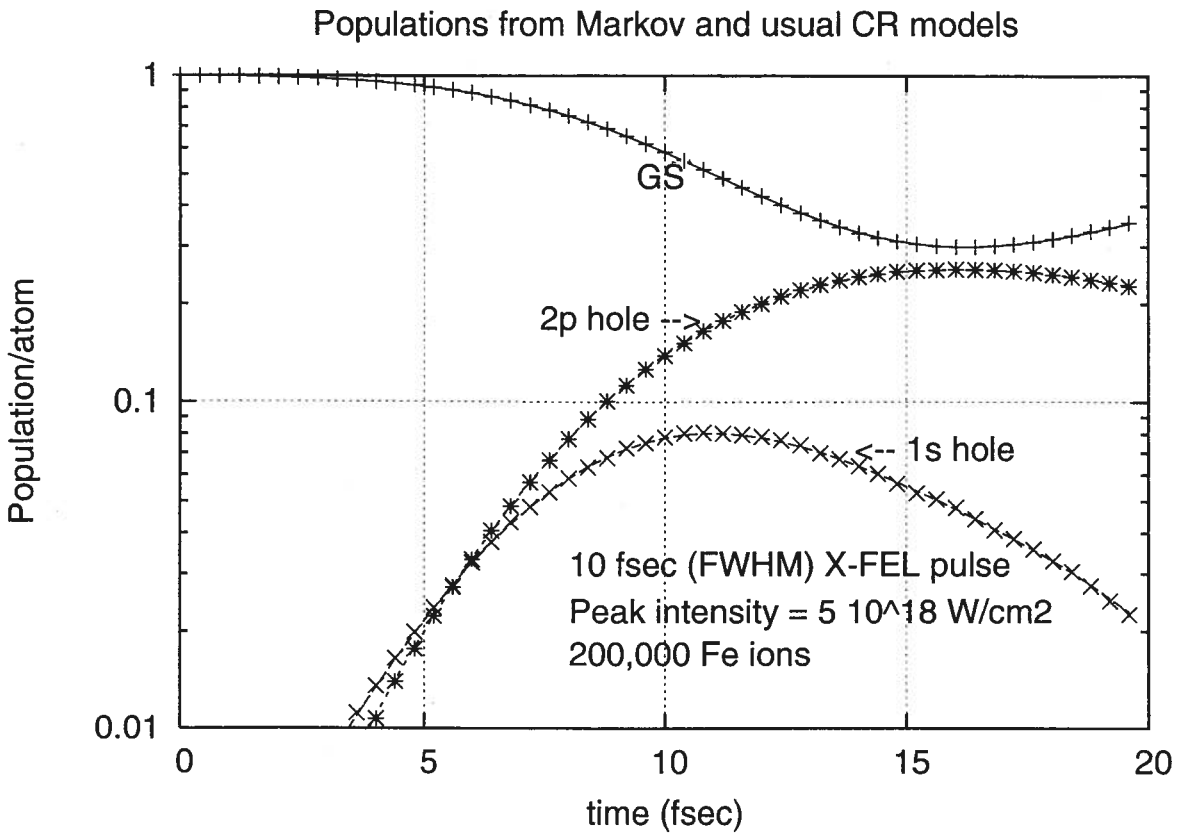

Fig. 5-1.) Time-dependent populations from Markov (points) and usual CR model (curves). The populations agree closely. The Markov calculation is performed for 200,000 Fe ions exposed to a 10 fsec XFEL pulse of peak intensity 5 10^{18} Watts/cm^2. The peak intensity occurs at t ~ 13 fsec. The groundstate (GS) population falls to ~ 0.3 and because the other states have much smaller absorption for the 7.1 keV XFEL photons, this implies a ~ 50% reduction in the absorption, i.e., bleaching. For times before ~ 10 fsec, these populations predict gain for the 1s-2p K_α transition.

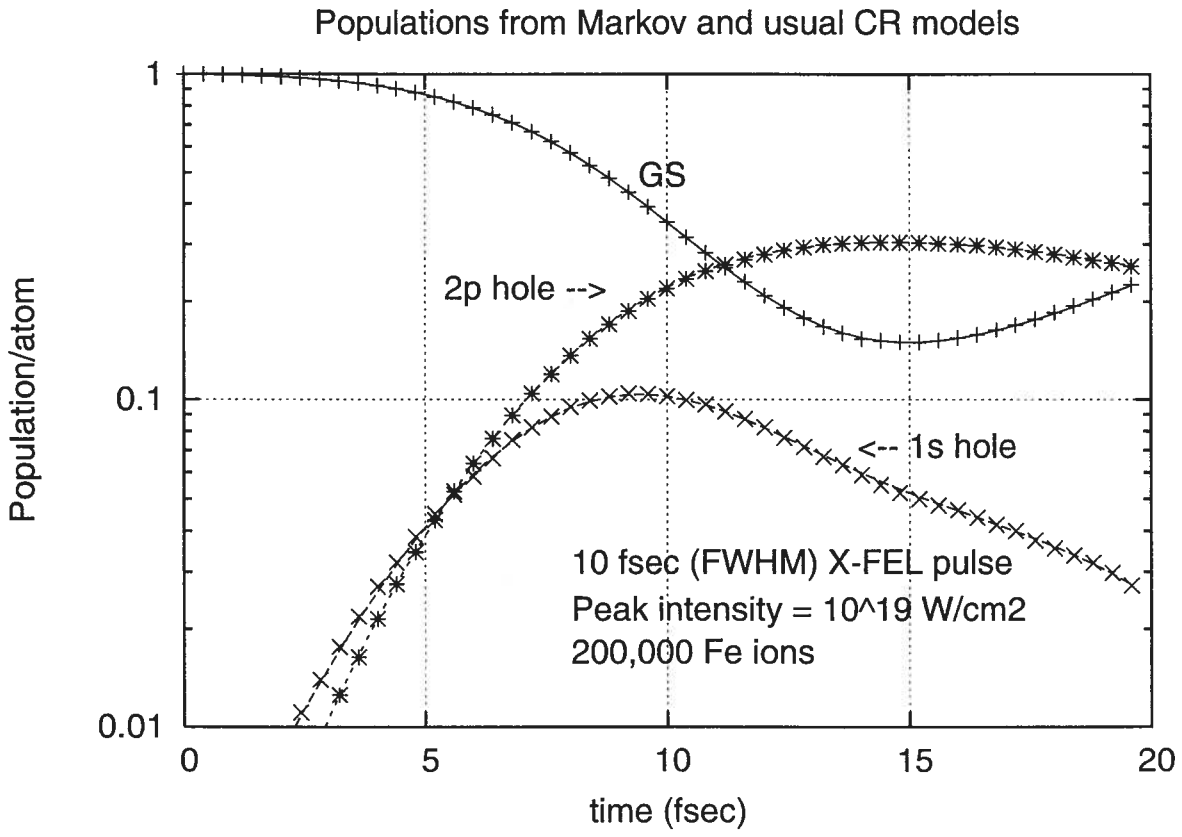

Fig 5-2.) Populations for peak XFEL intensity = 10^{19} W/cm^2. Again the Markov CR (points) agree with the usual CR (curves).

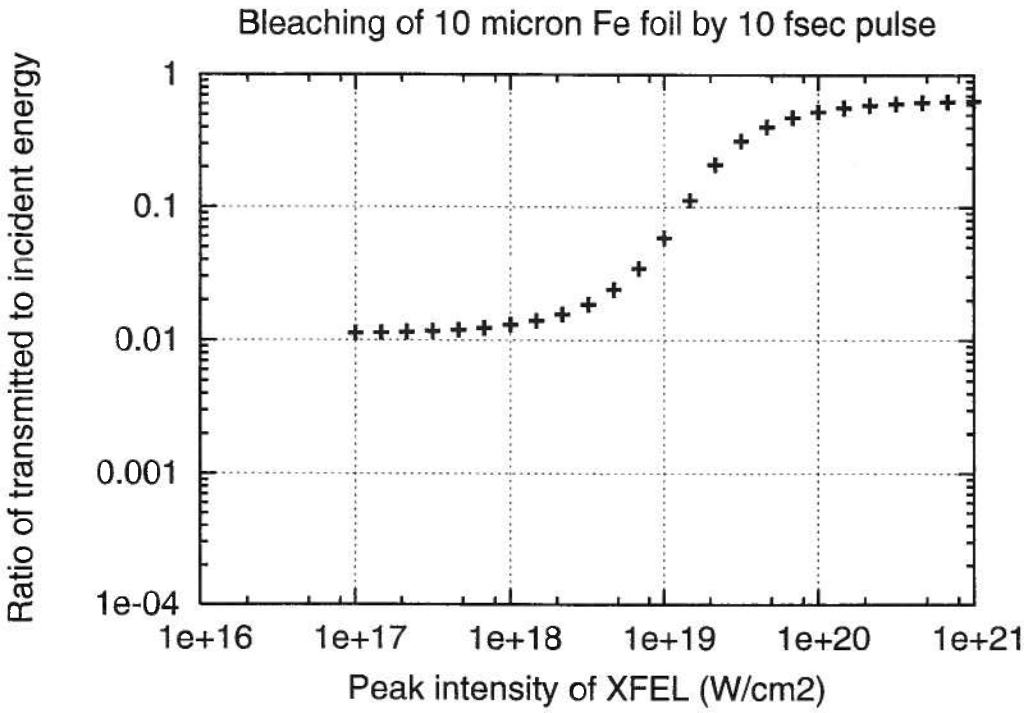

Fig. 5-3.) Raytrace calculation for bleaching of a 10 micron foil target. The transmitted energy/density fraction is plotted as a function of the incident X-ray pulse peak intensity.

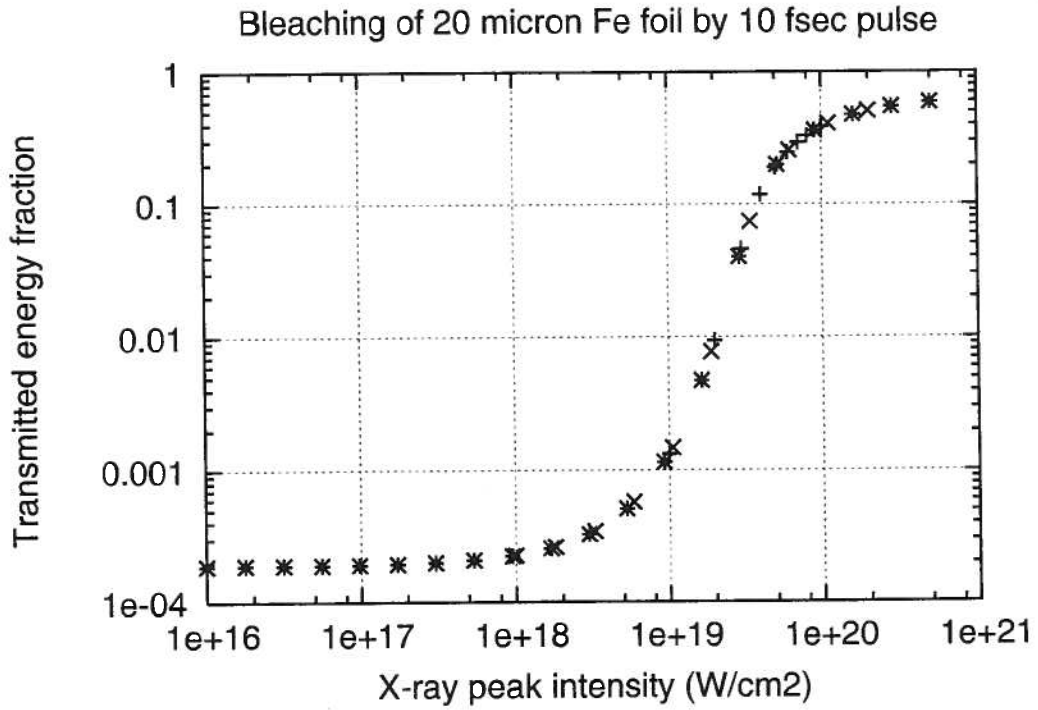

Fig. 5-4.) Raytrace calculation for bleaching of a 20 micron foil target. These results are in approximate agreement with the SACLA experiments.

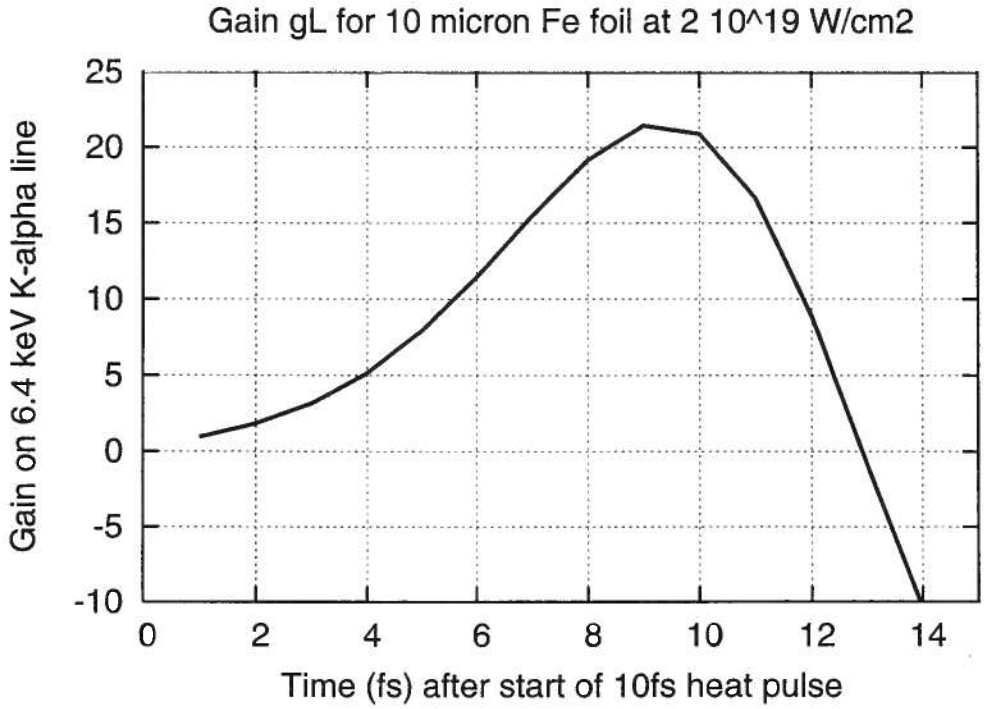

Fig. 5-5.) Total target gain for K_α emission from a 10 micron Fe foil irradiated at 2 10^{19} W/cm^2. The gain is calculated by the travelling-wave formula Eq. (6-3). The gain is strongly time-dependent and, consistent with the populations shown in Figs. (5-1, 5-2), is only positive for the first half of the heat pulse.

6.) Raytrace + CR for bleaching and gain

In this section we give the main equations used in the ray-trace code.

6A.) Modeling interaction experiments with ray-trace method

The ray-trace calculation is a one-dimensional solution of the radiation advection equation for the x-ray laser photons:

$$\frac{\partial I}{\partial t} = -c\frac{\partial I}{\partial x} - \alpha c I \qquad (6\text{-}1)$$

Here I = X-ray laser beam intensity (W/cm^2), c = speed of light and α = X-ray attenuation coefficient (cm^{-1}). The change in the atomic state caused by X-ray absorption changes the attenuation α, so $\alpha = \alpha(x, t, [I(x, t')])$ depends on the X-ray intensity at position x at previous times $t' \leq t$.

Equation (6-1) is solved together with the CR model for the atomic populations that determine the attenuation coefficient $\alpha(x, t)$.

For two-dimensional calculations, Eq. (6-1) can be solved along rays which are straight lines in (r, z) space; the rays lie on the surface(s) of a family of hyperboloids whose center is along the beam axis.

Non-neutral focal spot

In the context of the macroscopic geometry of X-ray target interaction, we can ask about the electrostatic environment for the Fe experiments. Since the X-ray pulse can ionize every atom in a tube of diameter ~ 50 nm through the 10 or 20 micron target foil, and produces photoelectrons or Auger electrons with energies $\geq$ 5 keV, it is possible to worry that the focal spot charges to a high potential. Indeed, a simple estimate based on the number of atoms in the interaction region implies a very high voltage (~ 10 keV) sufficient to confine the emitted electrons. We believe this would happen in an insulating target (although such a high voltage would surely cause breakdown inside the material). Such a high voltage cannot occur in a metallic target because the charge is neutralized by a return current as described in Appendix D.

6B.) XRL gain calculaton

We use populations from the atomic model to calculate x-ray laser gain. The instantaneous local gain coefficient g(x, t) is formed by the usual formula,

$$g(x,t) = \frac{A}{cg(\hbar\omega)\Delta\hbar\omega}\left(N_u - \frac{g_u}{g_l}N_l\right) \qquad (6\text{-}2)$$

The notation may over-use one letter of the Roman alphabet, but anyway,

$g(x, t)$ is the gain (= $1/I \; dI/dx$) for the X-ray intensity $I(x, t)$
$g(\hbar\omega)$ is the photon density of states at the X-ray energy
g_u, g_l are statistical weights of upper and lower levels
N_u, N_l are atomic populations for those levels at x, t
A is the Einstein A-value for the transition u --> l
c is the speed of light in vacuum

An important point about Eq. (6-2): the gain can be positive without requiring $N_u > N_l$. If $N_{1s} = N_{2p}$, that is already an inverted population. Figures in section 5 show this is exactly the case for the XFEL irradiation.

6C.) Traveling-wave gain calculation

The XFEL pulse is 10 fsec long, and has a spatial extent of 3 microns. For a 10 or 20 micron target, this pulse crosses the target like a stretch limousine driving through a tunnel. If one calculated the gL ("gain-length") product as a simple integral of the instantaneous local gain $g(x, t)$ as

$$\int g(x,t) \; dx$$

the result would always be negative because the target does not simultaneously have gain at front and back surfaces.

The proper calculation follows a hypothetical seed beam that enters the front surface at some start-time t_o. The traveling-wave gL product is

$$gL = \int g(x - c(t - t_o), \; t) \; cdt \qquad (6\text{-}3)$$

Here it is assumed that there is no sensible difference in propagation velocity (= c, the vacuum speed of light) between the seed beam (K_α radiation in our case) and the main XFEL pump beam. If there were such a difference, the foil targets would only show gain for thin foils.

The start-time t_o could be early or late relative to the main pump pulse, and in an experiment it is most likely that the seed pulse is long enough to require an integral over t_o. The high-gain parts of this integral will be dominant in the emitted XRL pulse.

We compared calculations of gL for thick and thin foils and found the integral is accurately linear in foil thickness.

7.) Super-radiance

From the beginning of this project we have suspected that the poorly-known phenomenon of super-radiance could be important for X-FEL experiments. Super-radiance is a spontaneous coherent decay process in which a number of identical excited atoms de-excite in phase at a rate that can be enormously larger than the independent incoherent rate (which is the usual emission rate). For the XFEL, the pump X-ray beam does produce a large number of excited atoms within a short time.

An essential criterion for super-radiance is that the radiative line-width should be no larger than the actual line-width. In most plasmas the radiative (natural) line width is much smaller than Stark, collisional or even Doppler width, and super-radiance plays no important role. However for the Fe or Cu XFEL targets, the Auger decay rate is about equal to the radiative rate, so the criterion for super-radiance seems to be met for Fe or Cu XFEL targets.

The papers or books dealing with super-radiance are not simple; it is a coherent-optics many-body effect and elaborate theory is natural. With some difficulty, we have discovered that collisional broadening is not treated in the most popular of the reference works. We have therefore set outselves the challenge of making a general theory of super-radiance including collisional broadening and, hopefully, in a form suitable for computational implementation. While we made progress toward this goal (equations are summarized in Appendix B) this part of our project is not complete.

The method we adopted is to write kinetic equations for the linear-combination populations which are the "coherent" superposition states for few-atom systems. The coherent superpositions are mixed by collisions and the coherent emission is destroyed when the collision rate is sufficiently large, i.e., when it is comparable to the radiative rate. We intend to continue these calculations and we are discussing the possibility of an experiment intended to look for super-radiant emission in X-FEL target interactions.

REFERENCES

1.) R. H. Dicke, "Coherence in Spontaneous Radiation Processes", Phys. Rev. **93**, 99 (1954).

2.) C. Cohen-Tannoudji, J. Dupont-Roc and G. Grynberg, **Processus d'Interaction entre photons et atomes**, Editions du CNRS, 1988.

3.) R. Rohlsberger, K. Schlage, B. Sahoo, S. Couet and R. Ruffer, "Collective Lamb Shift in Single-Photon Superradiance", Science **328**, 1248 (2010).

4.) R. Rohlsberger, H.-C. Wille, K. Schlage, B. Sahoo, Nature **482**, 199 (2012).

5.) M. Gross and S. Haroche, Physics Reports **93**, 301 (1982).

8.) Molecular Dynamics with quantum atomic kinetics

Molecular dynamics (MD) is based on classical mechanics for atomic motion and the atomic kinetics (CR or Collisional-radiative) makes an assumption equivalent to assuming the atomic state is measured on every time-step. This assumption is usual in atomic spectroscopy but neglects a class of quantum atomic interference effects. The question we address here is " *Is a more rigorous calculation too demanding for normal workstation computers?* "

The feasibility question was whether one-atom quantum interference effects could be calculated in a many-atom code. We studied line profiles for hydrogen lines, combining the Schroedinger equation with simple MD. The code could handle 300 atoms with 13 excited states (n = 2, n= 3 states) on each atom. The atomic states are described by a density matrix (details are given in Appendix C). For this purpose an existing one-atom Schroedinger equation code[1,2] was converted into a many-atom code as proposed in reference 3. The combined code was used for a test-calculation of the Stark profile of hydrogen atoms moving in the presence of a singly-charged Fe impurity. The calculation was appropriate to a gas of atmospheric density at a temperature of ~ 0.5 eV. Because the hydrogen atoms move with thermal velocities ~ 6 10^5 cm/sec, they experience time-dependent electric fields $\mathbf{E}(\mathbf{R}_j, t)$, where $\mathbf{R}_j(t)$ is the position of the j^{th} hydrogen atom. The calculation we have performed is not sufficiently realistic to be of research interest in itself, but illustrates the kind of calculation that can be performed by a many-atom Schroedinger code (and not easily performed otherwise).

The computational questions: is the data storage requirement feasible? Is the run-time small enough that the code could be used on a normal workstation computer? The calculations performed give affirmative answers to these questions, but better results could be obtained from larger or faster computers.

In the CR model, the quantum states {j} are a pre-determined set of eigenfunctions of the one-atom Hamiltonian. The CR model can calculate the average populations N_j of these states and can calculate transitions between the states using transition rates calculated by quantum mechanical collision theory. However the CR model has no way to describe linear combinations of the states.

For example, if a hydrogenic atom is placed in a local electric field $\mathbf{E}(r, t)$, the 2s and 2p states actually form linear-combination states with dipole moments oriented at various angles to the electric field. If the electric field is time-dependent, this linear combination evolves in a complicated way entirely outside the scope of the CR model. The best that CR can do is describe the resulting Stark splittings and shifts by an overall Stark line-profile.

Another interesting example is the Collisional suppression of Doppler broadening[4]. In the CR model the emission is an instantaneous event and the emitted line frequency reflects at most the instantaneous velocity of the atom (ion). However a quantum calculation shows the emission occurs over a substantial time (~ nsec for

hydrogen) and during that time there could be collisions which cause the emitted line to be frequency-modulated in a way that narrows the central portion of the line-profile. This effect can be calculated separately and then grafted onto the CR line-profiles, but such a procedure is not very satisfactory. These line-profile questions are a central issue for plasma opacity. The Schroedinger + MD combination is a new way to address basic questions about radiation coupling to matter.

Computation results and times

We attach figures showing the Stark profile calculations with different numbers of ions. The more ions, the less numerical noise in the results. The key question is how much computer time is required. For the calculations shown the computer times were:

3 atoms 18 minutes 30 atoms ~ 5 hours 300 atoms ~ 53 hours

These calculations were performed with equal run times (60 psec), equal time steps (dt = $2\ 10^{-17}$ sec) and equal resolution of the spectrum (1000 photon frequencies). The Fourier inversion to produce the spectrum uses a significant fraction of the computer time; we used a home-made "semi-fast Fourier transform".

The computer code described here is a *general tool* which could be used to check and improve line broadening theory if the treatment of atomic motion, collisions and pair potentials were appropriately improved. The code can study difficult issues like the theory of collisional suppression of Doppler line-broadening.[4]

In the past this Schroedinger code was also used to predict nonlinear response to high-power X-rays. The X-rays were modeled as a coherent EM field of very high frequency. The predictions included multiphoton absorption, harmonic generation and Rabi oscillations.

REFERENCES

(1) "Electromagnetic Waves", R. More, T. Kato, Y.S. Kim and M. G. Baik, Chapter 13 in **Plasma Polarization Spectroscopy**, Ed. by T. Fujimoto and A. Iwamae, Springer, Berlin, (2008).

(2) "Atomic Processes and High-Power Laser Radiation", R. More and H. Yoneda, in Science of Super-strong Field Interactions, p. 139, Ed. by K. Nakajima and M. Deguchi, AIP Conference Proceedings, vol. 634 (2002).

(3) R. More and F. Wang, "**Molecular dynamics with atomic transitions and nuclear reactions**", 24th IUPAP Conference on Computational Physics (IUPAP-CCP 2013), Journal of Physics Conference Series **454**, 012027 (2013).

(4) D. Burgess, D. Everett and R. Lee, J. Phys **B12**, L755 (1979).

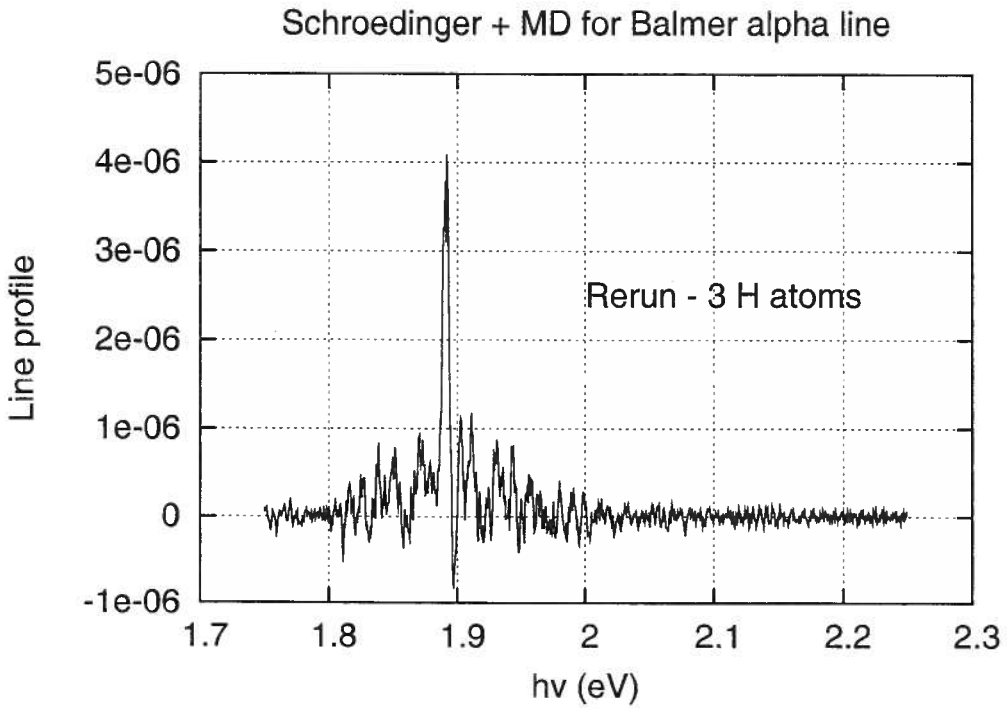

Figure (8-1) Balmer alpha line-profile for a 3 atom calculation using the Schroedinger + MD method. The atoms move in the presence of a single charge +e and in their reference frame the perceived electric field is time-dependent.

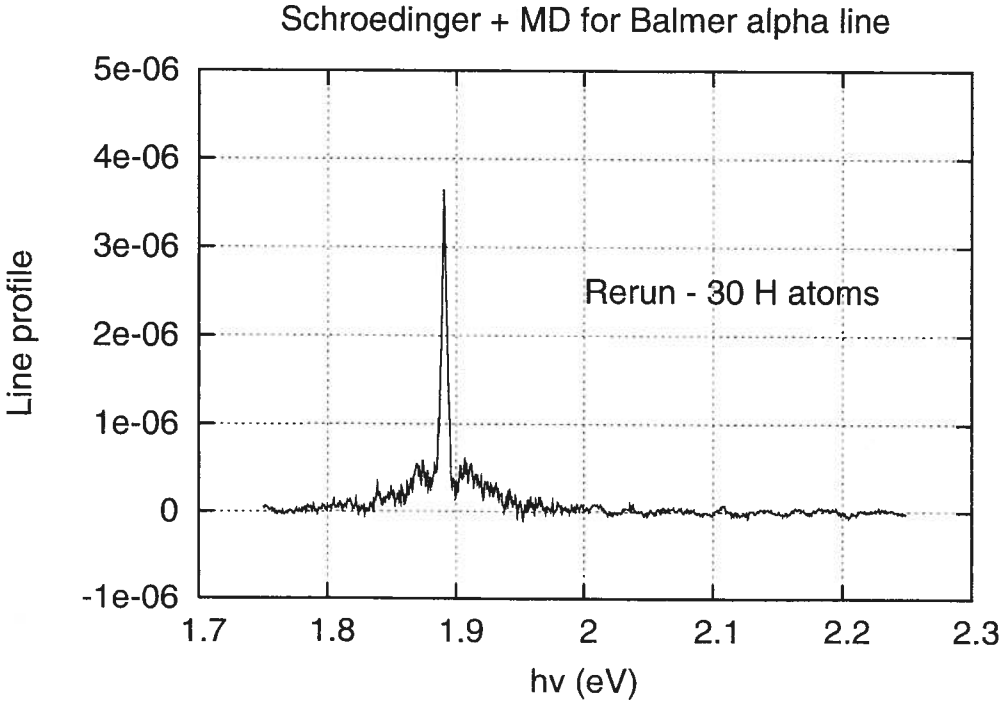

Figure (8-2) Balmer-alpha line profile for a 30 atom calculation at the same conditions.

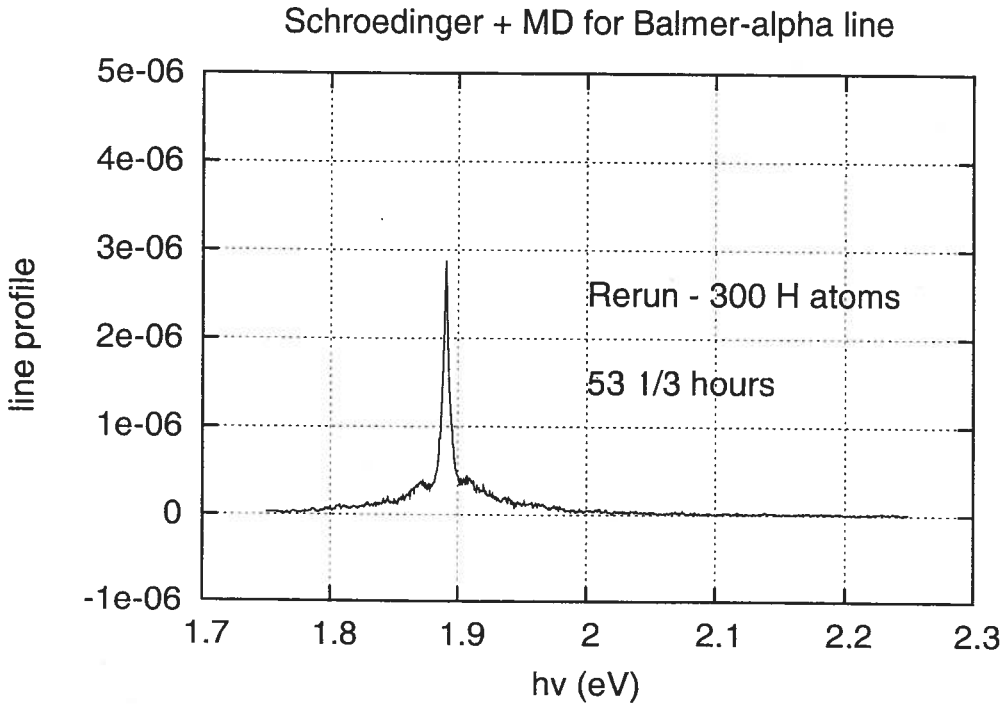

Figure (8-3) Balmer alpha line-profile for a 300 atom calculation using the Schroedinger + MD method. The line splitting is caused by atoms moving in the presence of a single charge +e; the atoms experience an electric field which changes magnitude and direction as the atoms move.,

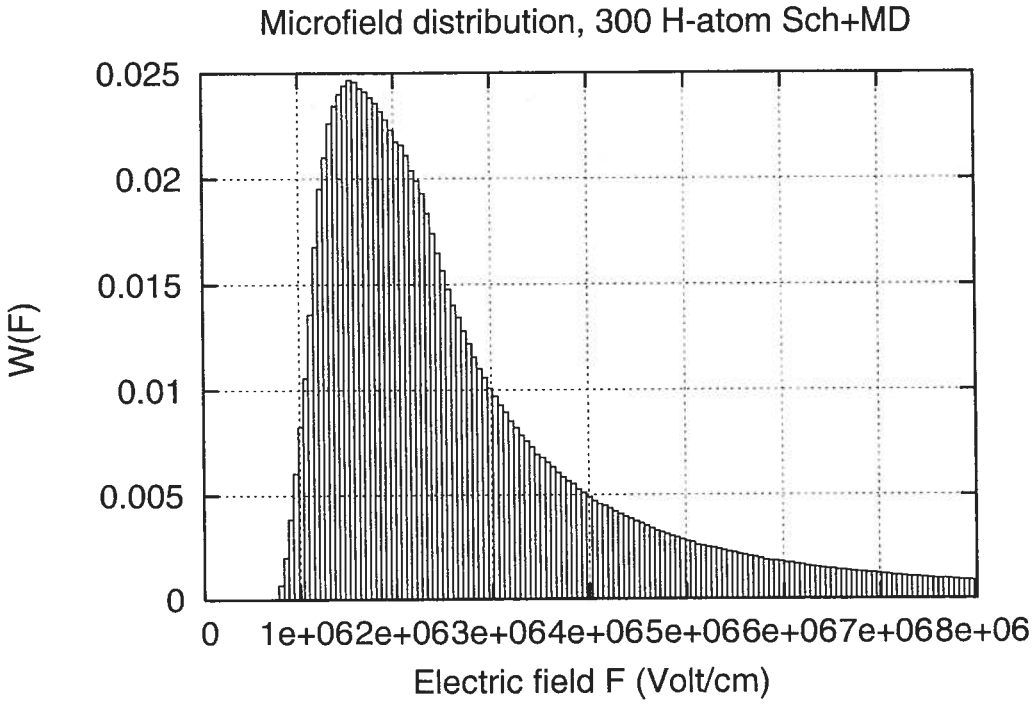

Figure (8-4) Histogram of electric fields experienced by the atoms in the 300-atom calculation.

9.) MD + CR

The purpose and method of the MD + CR calculation has been thoroughly described in the preceding sections. Here we simply show some results from the complete calculation.

The calculation describes a small volume in the focal-spot of the XFEL. This region is understood to be surrounded by plasma at similar conditions and is therefor treated using periodic boundary conditions; however energetic Auger electrons and energetic fluorescence radiation are assumed to escape.

The particle motion begins with 21296 Fe ions in a bcc lattice (a-Fe). The atoms are essentially confined in their lattice positions by a pair force which is adjusted to preserve the correct solid density. As they ionize under the influence of X-ray irradiation, the atomic forces are overwhelmed by Coulomb repulsions based on the calculated instantaneous ion charges. The atoms move to a disorderly arrangement due to the random changes in their charge states. Figures (9-1) and (9-2) show the ion positions in a small corner of the simulation box.

The atomic kinetics is treated by the "Markov CR" method discussed in previous sections and tested in section 5. Figure (9-3) shows the populations of four states of the Fe ions. As in the simpler calculations of section 5, it is evident there is an inversion on the 1s --> 2p transition for the first part of the X-ray FEL heat pulse.

Figure (9-4) shows the numbers of Fe ions in different charge states at different times during the calculation. The assumed recombination rate is rapid enough to prevent an accumulation of high charge ions, but it is not certain that this recombination rate is physically correct and further study is needed on this important point.

The target heats during the X-FEL interaction. It absorbs more than 7 keV per atom from the FEL. However much of this energy is spread by multi-keV Auger electrons and fluorescence radiation over a 1-micron tube around the XFEL interaction region. By adding up the energies of low energy electrons, produced by certain Auger transitions and by three-body recombination, we estimate that the target interaction region reaches a temperature ~ 100 eV at the end of the XFEL pulse.

For our gain calculations we use a constant line-width close to the observed K_α line-width (6 eV). If the target is heated to 100 eV during the XFEL interaction the line-width should be considerably larger late in the pulse, but by that time the gain is already reduced to small or negative values by the changes of atomic populations.

Of course the central question for this feasibility study is whether these calculations could be performed. The figures show that the answer is affirmative.

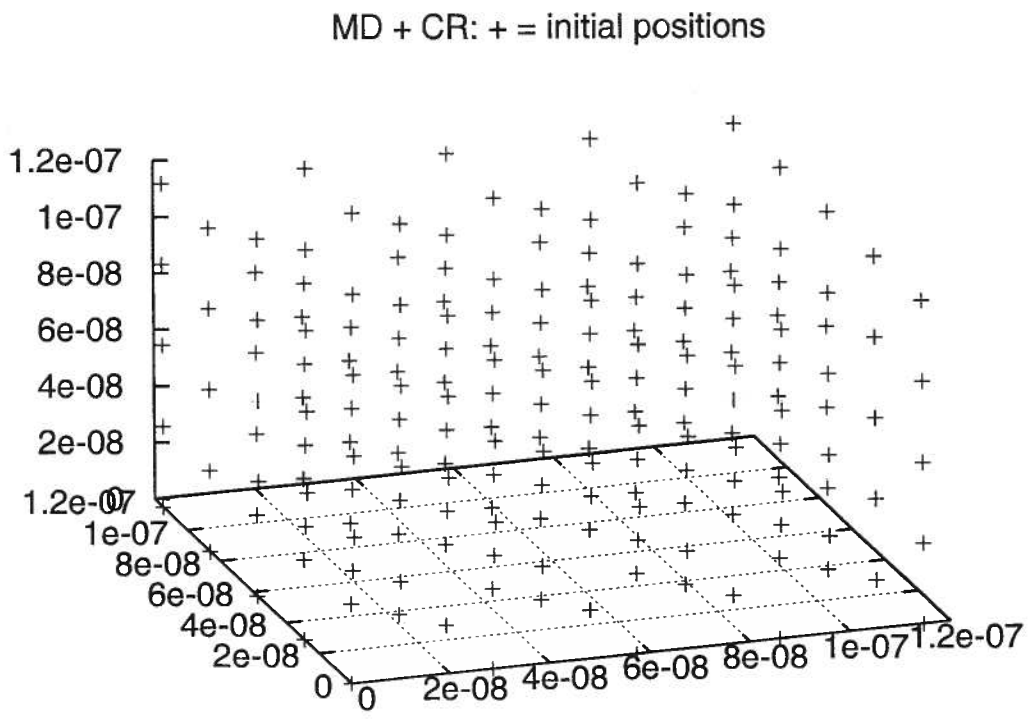

Figure (9-1) Initial positions of Fe atoms (bcc lattice) in the lower-left corner of the simulation cell.

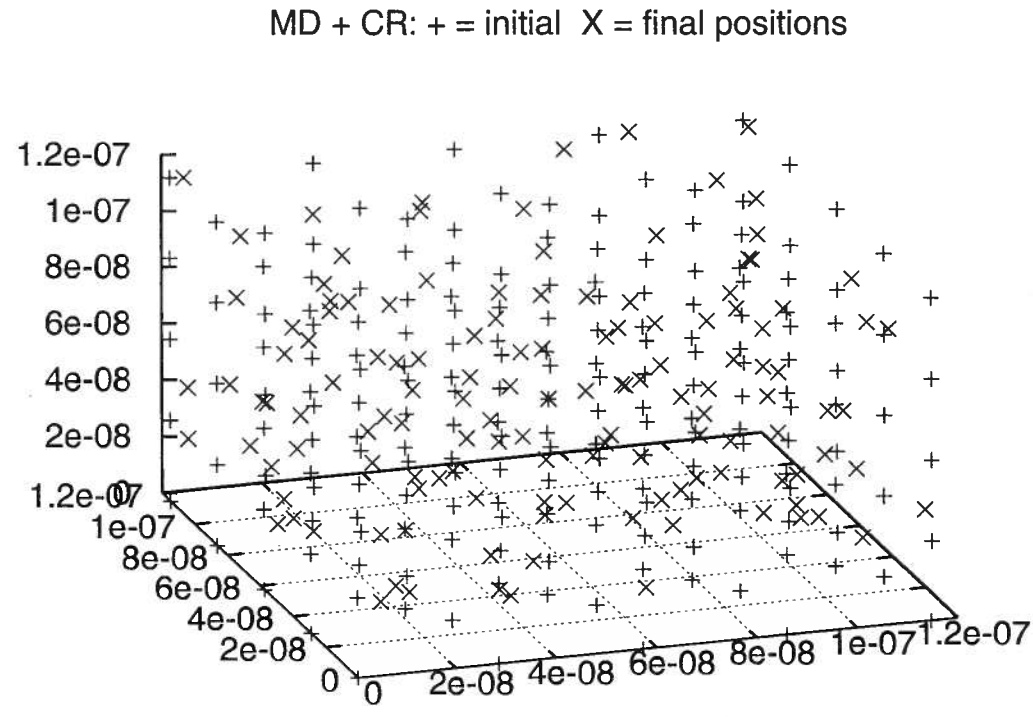

Figure (9-2) Final positions of atoms (ions) in the same spatial region. These are not necessarily the same ions because the ions are free to move.

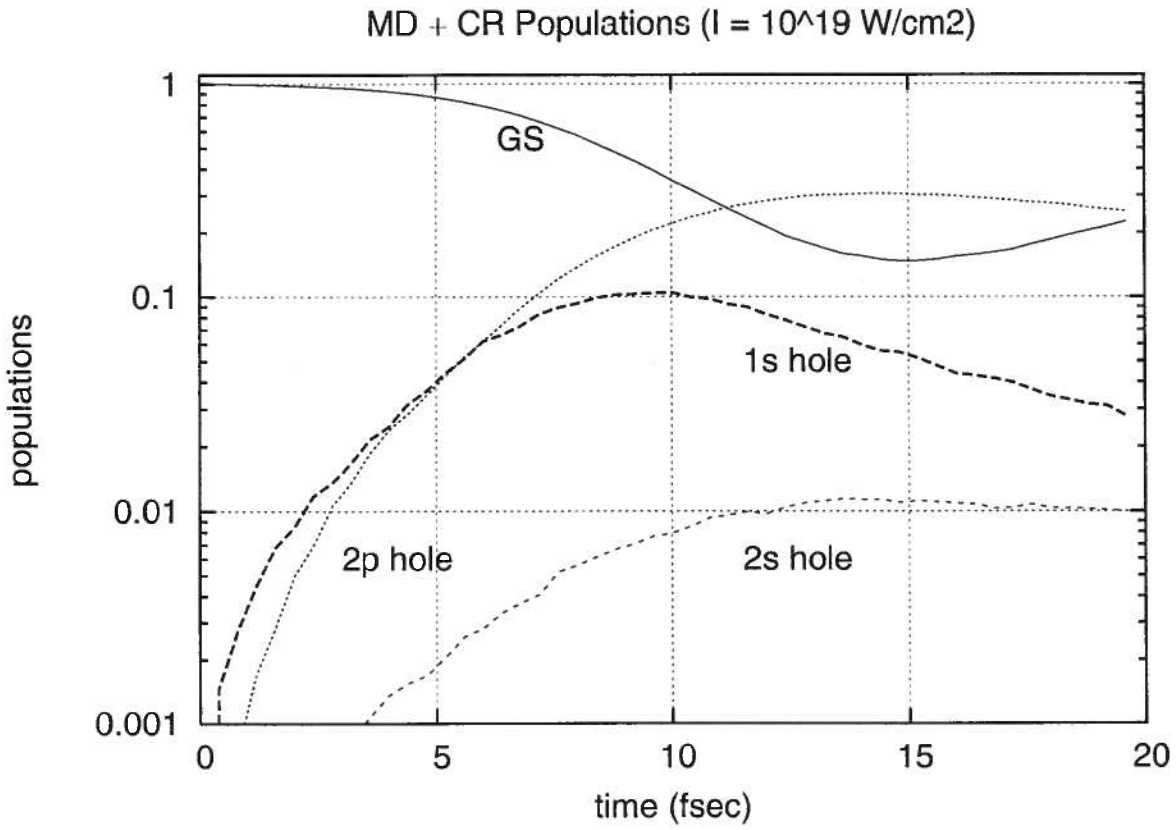

Figure (9-3) Populations for groundstate neutral Fe ("GS") and 3 excited states during MD + CR calculation of irradiation by a 10^{19} W/cm^2 Gaussian pulse of 7.1 keV X-rays. The pulse peak intensity occurs at about 13 fsec. The populations are consistent with an early time inversion on the Kalpha transition.

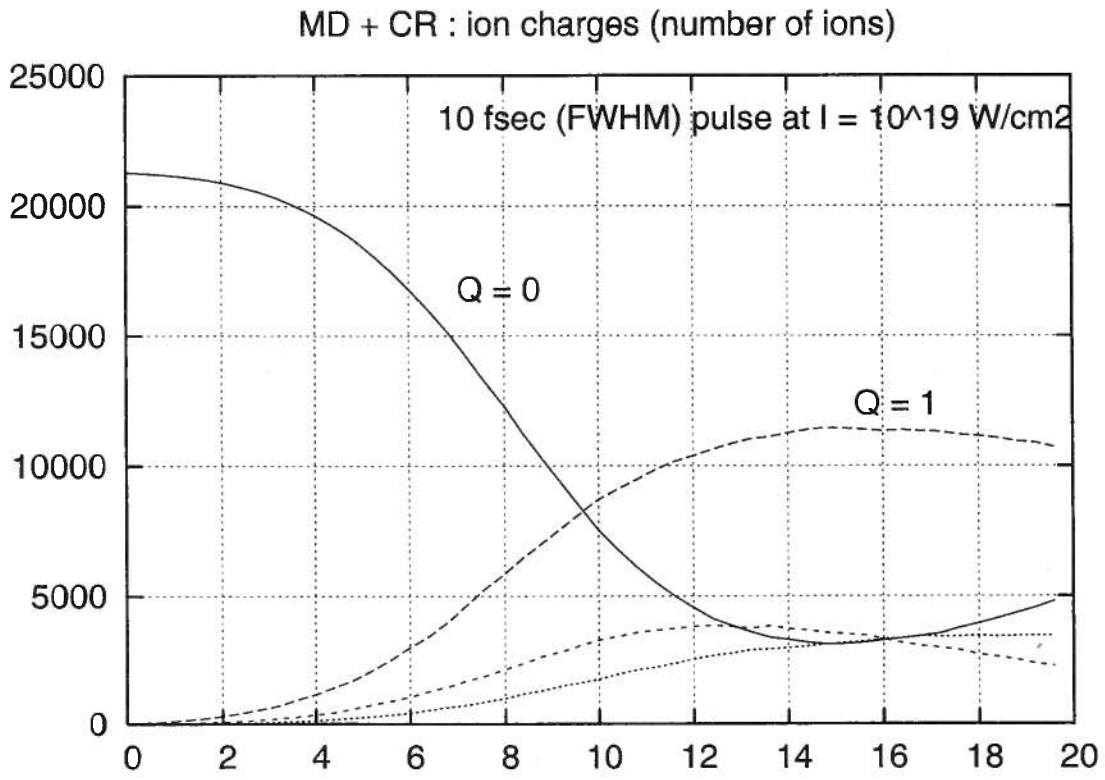

Figure (9-4) Numbers of Fe ions in different charge states during the MD+CR simulation (same case as Fig. 9-3). Neutral (Q = 0) and 1+ ions are marked and the 2+, 3+ ions should be easily distinguished: the 2+ ions are produced somewhat earlier in the pulse.

10.) Feasibility: a summary

For this project, we have written first versions of computer codes, which can be used to analyze and predict a new class of experiments that are possible using the new high intensity x-ray FEL sources. The codes give results consistent with experiments already performed at the SACLA X-FEL facility. The phenomena examined so far are x-ray induced nonlinear transparency (factor 10 increase in x-ray transmission through a foil with few fsec switching time) and pumping of a saturated inner-shell x-ray laser.

This type of laser is of unique practical interest for several reasons:

1.) With x-ray energies of 6-8 keV, it gives a coherent source matching the x-rays used for many years for medical and dental diagnostics, so that people know how to interpret the images that can be made with this source.
2.) The targets that emit the x-rays are simple flat foils and are driven (pumped) by a single short pulse. They can easily be irradiated in a high rep-rate mode.
3.) Output x-rays from a saturated laser K_α are a coherent source suitable for a wide range of quantum optical applications, holography, interferometry, etc.

The feasibility issue we addressed in this project is computational: is it possible to combine molecular dynamics particle simulation with collisional-radiative (or more elaborate) atomic modeling, and do so on a modest table-top work-station computer? Our answer is entirely affirmative and in fact we have done so.

The computer codes we have written are exploratory and not yet mature modeling tools. Many questions remain open and we have not yet explored the wide range of atomic/plasma phenomena which could be described by a many-atom atomic kinetics code. However the codes we have written open the door to this research.

For computer codes, "feasibility" means that the code can be written and that it can be used with reasonable demands on human and computational resources. The codes we describe in this report are of the order of 20-50 pages long and have run-time on workstation computers of a few minutes to a few hours. By any standard the calculations are feasible, given the numbers of atoms (ions) used, which range from a few hundred atoms for the MD + Schroedinger code to 800,000 atoms for the Markov CR code described in sections 5, 6.

11.) Future experiments and future codes

One can confidently predict that X-FEL research has a strong future with many applications to pure and applied science. X-FEL facilities are now under construction in four countries.

There is a question which facility will take the lead and which applications will be most effectively pursued. LLNL has a deep fund of experience with X-ray lasers and related radiation science (LLNL Lab Reports were originally called "UC Radiation Lab" reports). LLNL also has a strong history of top-quality scientific computation.

We will propose an extension of this project during FY14 with the main goal of helping to nucleate LLNL activities to perform new science on existing X-FEL facilities. Other scientists inside LLNL have strong interest in this subject (we could quote from a large collection of e-mails). However in the current difficult funding environment an inexpensive and cooperative project is the most that can be hoped for. Our proposal for continuing the project will include the following activities:

1.) Edit a compilation of LLNL research publications on X-ray laser science during the years since the first Laboratory X-ray laser, achieved at the LLNL Nova laser in 1985. TID estimates that this would cost about $4000 or $5000.

2.) Extend the existing computer codes to treat Cu target interactions. Cu is being used in the most recent experiments in SACLA.

3.) Organize (through meetings in the Lab) a group who will propose a campaign of X-FEL experiments at LCLS during FY15. This group would seek outside funding for effort to develop x-ray laser applications including medical applications of holography.

Having a demonstrated ability to model and design such X-FEL experiments is likely to be a persuasive argument in favor of that research program. The MD + CR codes give more powerful modeling than anything available in other Labs at the present time.

ACKNOWLEDGEMENTS

This project was assisted by a number of people whose help should be acknowledged. Dr. Feilu Wang of the Beijing Astronomical Observatory performed numerical calculations of atomic rates and participated in discussions of many aspects of the physics. Dr. Jonathan Wurtele of UC Berkeley Physics Department provided advice on modern free-electron laser technology. Dr. Hitoki Yoneda, Director of the Institute for Laser Science in the UEC Tokyo showed us the unpublished results of his experiments at SACLA and discussed theory and experiment in great detail. Dr. William Goldstein, Deputy Director of LLNL, provided support and encouragement and drew our attention to important research papers on XFEL target interactions. Drs. Stephen Libby, John Barnard, James Dunn gave detailed comments on various ideas and provided useful references. Stefan Hau-Riege and John Barnard made interesting comments about the electrostatic potentials in the XFEL targets. Lynn Heimbucher at LBNL helped for finding safe lodging and proper badges and permits for Dr. Wang and her family.

Appendix A.) Atomic Data for Fe

We give some examples of atomic rates and describe some tests we used to evaluate the FAC data set.

Radiative transitions of one-hole core states in Fe^+:

1s --> 2p	A = 5.428	10^{14} sec^{-1}
1s --> 3p	6.374	10^{13}
2s --> 2p	1.586	10^{11}
2p --> 3s	2.770	10^{11}
2p --> 3d	2.877	10^{12}
2s --> 3p	3.86	10^{12}
3s --> 3p	4.51	10^{10}
3p --> 3d	8.95	10^{10}

Several points deserve comment: first, the rates are consistent with the usual selection rules; second, transitions between shallow hole states (3p, 3d) have smaller rates; third, there are many transitions involving the partially-filled 3d shell and we only give the average rate for these transitions. In the free neutral atom the 3d shell has four holes (in some of the lowest-energy states) and those states support orbital angular momenta up to 6 or spin angular momentum up to 2 (but not at the same time). This structure is "quenched" by the potentials of the neighbor atoms in metallic iron. Fortunately the chief interest in the first X-ray laser experiments will be in deeply bound states (1s, 2s, 2p) whose behavior is less delicate.

The reader who is surprised at the direction of the arrows (for emission) should remember that these are hole states, i.e., in the first transition listed, a 2p electron emits an energetic photon while filling a hole in the 1s shell, represented as a transition of the hole from 1s to the 2p shell.

Radiative transitions involving 2-hole core states:
The data-set includes many radiative transitions such as $2s^2$ --> 2s2p, $2s^2$ --> 2s3p, 2s2p --> $2p^2$, 2s2p --> 2s3s, 2s2p --> 2s3d, 2s2p --> 2p3p, $2p^2$ --> 2p3d, $2p^2$ --> 2p3s, 2s3s --> 2s3p, 2s3s --> 3s3p, 2s3s --> 2p3s, 2p3s --> 2p3p, 2p3s --> $3s^2$, 2p3s --> 3s3d, 2s3p --> 2s3d, 2s3p --> 2p3p, 2s3p --> $2p^2$, 2p3p --> 2p3d, 2p3p --> 3s3p, 2p3p --> 3p3d, $3s^2$ --> 3s3p, 3s3p --> 3s3d, 3s3p --> $3p^2$, 3s3d --> 3p3d, $3p^2$ --> 3p3d and 3p3d --> $3d^2$.

We give details for a few of the transitions:

$2s^2$ --> 2s2p	A = 2.77	10^{11} sec^{-1}
$2s^2$ --> 2s3p	8.77	10^{12}
2s2p --> $2p^2$	1.06	10^{11}
2s2p --> 2s3s	3.16	10^{11}

These rates can be compared to the rates for the one-hole transitions given above and the comparison is a useful test of the FAC data. One can expect that the first case, $2s^2$ --> 2s2p should be related to, if not identical with, the 2s --> 2p single-hole transition. In fact the rates *agree to within a few percent* after corrections are made for

a.) In the 2-hole case two transitions contribute (a factor 2!).
b.) The radiative rate (A-value) is proportional to the transition energy $(\hbar\omega)^3$ which is slightly smaller for the two-hole transition (this factor is a 25 % change in the rate).
c.) In performing the comparison it is best to use the data for 2s --> $2p_{1/2}$, 2s --> $2p_{3/2}$ before the sum/average over initial and final states.

Similar analysis of a second case $2s^2$ --> 2s3p gives a similar result. In this case it was useful to separate the $3p_{1/2}$ and $3p_{3/2}$ transitions. The rate for 2s --> $2p_{3/2}$ is smaller by a factor 1/1.86 due to the spin change (both for 2s --> 2p and for $2s^2$ --> 2s2p) and including the factor ω^3, the rates then match to about 2 %.

We made similar comparisons of rates for 2s --> 2p and 2s2p --> $2p^2$, 2p --> 3s and 2s2p --> 2s3s, etc. The comparisons were very satisfactory except when 3d electrons were involved; the partly-filled 3d shell has a complicated structure.

These examples verify that the radiative rates from the FAC data-set are satisfactory.

4-level model for ray-trace calculations

At the beginning of this project, the first ray-trace code was combined with a four-state atomic model that calculates Fe inner-shell populations:

N_0 = ground-state neutral Fe
N_1 = state with one K-shell hole
N_2 = state with one L-shell hole
N_3 = state with two L-shell holes

Transitions between the four states are controlled by approximate cross-sections. Atomic processes include: Autoionization from M, L shells, Radiative transitions (M --> L, L --> K) and X-ray absorption from K and L shells. The results from this crude model already approximately agree with the experiments.

48 level for MD+CR

Our data-set of atomic rates for Fe core states was generated using the FAC code[(1)] by Dr. Feilu Wang, visitor to the UC Berkeley Physics Department group of Professor Jonathan Wurtele. The extensive list of transitions was simplified by keeping transitions having large rates above 10^{12}/sec. Since the entire laser-target interaction occurs in about $\sim 2\ 10^{-14}$ sec, processes with rates smaller than 10^{12}/sec will have little effect. The FAC code describes its one-electron basis states using relativistic jj coupling. For our purposes, this is more detail than necessary. We use a simpler description based on principal quantum number and orbital angular momentum. With this description, 48 levels suffice to describe the main 1, 2 and 3 core-hole states.

The overall goal of the LDRD feasibility project is to combine a collisional-radiative (CR) atomic model with Molecular Dynamics (MD) particle simulation and once these are successfully combined, various parts can be altered. For example, an improved atomic model could replace the data-set described here. The project is focused on understanding the SPring-8 X-ray laser interaction experiment on Fe targets and we use the conditions of that experiment to limit the scope of our atomic model. Future applications will require larger or more comprehensive atomic data-sets.

Appendix B.) Super-radiance in few-atom cluster

The original prediction of super-radiance by R. H. Dicke[1] seemed to show a possibility of enhanced radiative rates under certain conditions.

Not long after Dicke's paper, the experimental realization of maser and laser action raised interest in super-radiance, but by now it is generally believed that *stimulated emission* responsible for light amplification in lasers and the coherent phenomena of *super-radiance* are basically different, or at least, occur in different places in the formulas for emission of light[2]. Since the 1950's super-radiance has been observed in enough experiments to leave no doubt of the reality of the phenomenon, but it has probably not been observed in atomic transitions in a hot plasma environment. Recent nuclear (Mossbauer) experiments observed effects attributed to super-radiance[3,4]. The theory of super-radiance has been investigated for many years but apparently without addressing a key question about the effect of collisions on atoms emitting in hot plasma.[5]

The physics of super-radiance can be described as follows. The rate of emission of light during a transition from some initial state "i" to a final state "f" can be written

$$Rate_{i\to f} = \frac{2\pi}{\hbar}\left|H^r_{if}\right|^2 g(\hbar\omega) \qquad (1)$$

where

$g(\hbar\omega)$ = photon density of states ~ ω^2

$[n_\omega]$ = number of photons per mode

H_r = - (e/mc) $\mathbf{p}\cdot\mathbf{A}$ = matrix element for electron-photon coupling

Here A is the operator for the vector potential of a non-relativistic EM field,

$$A(r,t) = \sum_{k,\lambda} e_{k,\lambda} C_k \left(a_{k,\lambda} e^{ik\cdot r} + a^+_{k,\lambda} e^{-ik\cdot r}\right) \qquad C_k = \left(\frac{2\pi\hbar c^2}{V\omega(\varepsilon + \frac{\omega}{2}\frac{\partial\varepsilon}{\partial\omega})}\right)^{1/2}$$

The matrix element of H_r is easily transformed to a matrix-element of the dipole moment - e $\mathbf{r}$ (operator) for the radiating system. For a N-atom system H_r becomes the sum of the dipole moment matrix-elements of electrons on the N atoms. Eq. (1) calls for the square of the sum, rather than the sum of the squares, and that is the basis for the phenomenon of super-radiance. Eq. (1) is very general and the states "i" and "f" can be any stationary states of the many-atom system.

Stimulated emission is the enhancement of the emission rate due to the final state factor $[n_\omega + 1]$ which comes from the creation operator a+ in any one of the coupling terms. Super-radiance is an enhancement which occurs in a many-atom system when a transition occurs in such a way that the dipole moments of several atoms are coherent or in-phase. In this case, instead of a rate N times the single-atom rate, the rate is larger by a factor ~ N^2, where N is the number of atoms that participate. Super-radiance is not caused by any interaction between the emitters and may even be suppressed by any direct interaction, but rather is due to their common interaction with the radiation field.

We investigate the equations for super-radiance to decide two questions:

1.) Could it affect the results of the SPring-8 X-ray laser experiment on Fe targets?

2.) Could super-radiance be important in some other plasma radiative context so it should be included in the MD + CR computer code we will develop?

The original paper of Dicke makes highly idealized assumptions about the atomic system. The paper uses formal algebraic techniques based on the algebra of angular momentum operators. Dicke's calculation is most appropriate for nuclear magnetic resonance processes for which a simple spectrum of two levels (nuclear spin up, spin down) is realistic. In that case the interaction between the nuclear spins is very weak. Although Doppler broadening is mentioned in the paper, there is no detailed calculation of the effect of line-broadening.

Here we try to simplify the mathematics and test the assumptions to see if super-radiant phenomena can occur in a hot plasma HEDP context. Although we do not give a full treatment of all the mechanisms which can destroy the coherence responsible for super-radiance, it it is useful to list some candidates:

i.) For real atomic transitions, the excited states are typically degenerate. Even for the simpest case of emission by transitions 2p --> 1s, the initial upper level consists of 3 orbital states. However for the Fe XRL experiment, the 1s hole state produced by absorption of 7.1 keV X-rays is non-degenerate; it can radiate to any of three 2p states.
At very least, the effect of degeneracy is to dilute the super-radiance enhancement.

ii.) If two atoms are in different local environments, the degeneracy required for super-radiance might be lifted.

iii.) If the atoms are subject to electron-impact (or other) collisions, we expect the super-radiance correlations are destroyed. This is described by the equations given below.

We would like precise formulas to decide how much line-broadening is sufficient to destroy super-radiance, but we can also invoke common sense[5] to say that whenever the output photons from the two atoms are distinguishable (so we know which atom an observed photon came from), the super-radiance enhancement will be destroyed.

For level shifts, this common-sense criterion says that if the energies of excited states are separated by more than the natural (radiative) line-width, the super-radiance is reduced. For the effect of collisions, it also seems clear that super-radiance should disappear when the collisional line-width exceeds the natural (radiative) line-width. This estimate is supported by the model developed here. For the effect of degeneracy of the upper level, it seems clear that emission from different l,m states cannot be coherent when the photon polarization and direction are sufficiently different so that one can say which photon came from which atom.

For the Fe X-ray laser experiment we note that the short-pulse X-rays suddenly produce K-shell hole states in many Fe atoms in the target foil. The "upper" state for the following discussion is actually a 1s core hole state and the radiative "decay" is the transition 1s --> 2p of the hole. In the neutral Fe atom, the radiative rate is approximately equal to the Auger lifetime of the 1s state (the rates are approximately 5.4 10^{14}/sec in both cases). If super-radiance occurs, it would appear as an increase in the fluorescence yield, e.g., of 6.4 keV X-rays following absorption of the 7.1 keV pump.

The qualitative arguments do not give sufficiently precise formulas for occurance or absence of super-radiant enhancement of the rates, and we want to develop them further with computational models. The analytic and numerical calculation described here describes the collisional mixing of correlated excited states populated by emission from a single upper state. We work out the equations for a two-level two-atom system.

The kinetic model developed here for two atoms will show that the enhanced emission is suppressed by dephasing collisions. Consider two nearby hydrogen-like atoms in a plasma. Two-electron wave-functions involving 1s and 2p states may be constructed as:

State 1 = $\psi_{2p}(1)\,\psi_{2p}(2)$ (e.g., $2p^{+1} \sim Y_1^1$ for each atom)

State 2 = $(\psi_{2p}(1)\,\psi_{1s}(2) + \psi_{1s}(1)\,\psi_{2p}(2))/\sqrt{2}$

State 3 = $(\psi_{2p}(1)\,\psi_{1s}(2) - \psi_{1s}(1)\,\psi_{2p}(2))/\sqrt{2}$

State 4 = $\psi_{1s}(1)\,\psi_{1s}(2)$

The linear combination states (number 2 and 3 above) are appropriate if the basis states 1s(1) 2p(2) and 2p(1) 1s(2) have energies that are equal to within the natural linewidth.
In this case the radiative rates 1 --> 2 and 2 --> 4 are increased over the single atom rate γ by the coherence (= super-radiance). We give a simple analysis of the radiative rates based on the first-order perturbation theory which is quite accurate for radiative transitions because of the small size of the fine-structure constant.

For simplicity we omit the numerical coefficients. The square of the dipole matrix element from state 1 (from the list above) to state 2 is

$$\left|H_{12}^{r}\right|^2 \propto \frac{1}{2}\left|\left\langle\psi_{2p}(1)\psi_{2p}(2)\right|\ (r_1+r_2)\ \left|\psi_{1s}(1)\psi_{2p}(2)+\psi_{2p}(1)\psi_{1s}(2)\right\rangle\right|^2$$

The factor ½ comes from the normalization of the wave-function for state 2. Using the orthogonality properties of the wave-functions this can be simplified to

$$\left|H_{12}^{r}\right|^2 \propto \frac{1}{2}\left|\left\langle\psi_{2p}(1)\right|\ r_1\ \left|\psi_{1s}(1)\right\rangle+\left\langle\psi_{2p}(2)\right|\ r_2\ \left|\psi_{1s}(2)\right\rangle\right|^2$$

And this is then twice the one-atom matrix element, i.e., the radiation emission rate between these states is $2\,\gamma$ where γ = ordinary one-atom rate. The emission rate increases because the two atomic dipoles are in-phase for transitions 1 --> 2, 2 --> 4.
The rates are zero for radiative transitions 1 --> 3 and 3 --> 4 , because for those transitions (1 --> 3 and 3 --> 4) the transition dipoles are out of phase.

A more careful version of this calculation, using the formula for the vector potential operator, shows that the two terms have different phases with a relative phase (ratio)
which can be written

$$\exp(i\,\mathbf{k}\cdot\mathbf{\Delta R})$$

where $\mathbf{k}$ is the wave-vector of the emitted photon and $\mathbf{\Delta R}$ is the difference of position of the two atoms. If they are within one wavelength of each other, this factor is ~ unity. If they are farther apart, this phase factor is more interesting. It says that super-radiant enhancement can only occur

for atoms whose physical separation is transverse to the direction of observation (the vector **k** points toward the observer).

In a plasma, states 2, 3 can be mixed by collisions which make random changes in the phase of one or the other atom. We describe these as transitions 2 <---> 3 which occur with a rate σ. To order of magnitude, we expect $\sigma \sim$ linewidth/$\hbar$, so σ is much larger than γ for most plasma conditions. In many plasmas, even Doppler broadening exceeds the natural line-width. However, for inner-shell core hole states of Fe, the Doppler width is negligible, γ is approximately 5.4 10^{14}/sec, and the Auger decay rate is approximately equal to the radiative rate.

Rate equations for the atomic kinetics:

Dephasing collisions cause transitions between the equal-energy linear-combination states 2, 3. We describe the dynamics with kinetic equations for the linear-combination states. The equations written here assume there is no incident radiation.

The terms in brackets [...] are radiative transitions 1 --> 2 and 2 --> 4
The terms in braces {...} are the dephasing collisions 2 <---> 3:

$$\frac{dN_1}{dt} = -2\gamma N_1$$

$$\frac{dN_2}{dt} = \left[+2\gamma N_1 - 2\gamma N_2\right] + \left\{-\sigma N_2 + \sigma N_3\right\}$$

$$\frac{dN_3}{dt} = \left\{+\sigma N_2 - \sigma N_3\right\}$$

$$\frac{dN_4}{dt} = +2\gamma N_2$$

For a pair of atoms that start with both atoms excited (in state 1) $N_1(t) = \exp(-2\gamma t)$.
We solve the equations for N_2, N_3 by finding eigenvalues of the rate matrix. The solution can be written:

$$N_2(t) = A\left(e^{-2\gamma t} - e^{-\lambda_p t}\right) + B\left(e^{-2\gamma t} - e^{-\lambda_m t}\right)$$

$$N_3(t) = C\, e^{-\lambda_p t} + D\, e^{-\lambda_m t} + E\, e^{-2\gamma t}$$

$$\lambda_p = (\gamma+\sigma) + \sqrt{\gamma^2+\sigma^2} \qquad \lambda_m = (\gamma+\sigma) - \sqrt{\gamma^2+\sigma^2}$$

$$A = \left(\frac{\gamma}{\sigma} - \frac{1}{2}\right) + \frac{\sigma^2 - \gamma\sigma + 2\gamma^2}{2\sigma\sqrt{\gamma^2+\sigma^2}}$$

$$B = \left(\frac{\gamma}{\sigma} - \frac{1}{2}\right) - \frac{\sigma^2 - \gamma\sigma + 2\gamma^2}{2\sigma\sqrt{\gamma^2+\sigma^2}}$$

$$C = \frac{-\sigma A}{\sigma - \lambda_p} \qquad D = \frac{-\sigma B}{\sigma - \lambda_m}$$

$$E = -1$$

Solution of these equations gives

$$N_4(t) = (A+B)\left(1-e^{-2\gamma t}\right) - \frac{2\gamma A}{\lambda_p}\left(1-e^{-\lambda_p t}\right) - \frac{2\gamma B}{\lambda_m}\left(1-e^{-\lambda_m t}\right)$$

N_4 is the ground-state population, equal to the probability that two photons were emitted by time t.

For small σ, $N_4(t)$ is the super-radiance solution with its anomalously rapid emission:

$$N_4(t) = 1 - (1+2\gamma t)\, e^{-2\gamma t}$$

The physical reason for the "secular" term $\sim t\, e^{-2\gamma t}$ is that the rates 1 --> 2 and 2 --> 4 are exactly equal. N_4 reaches 90% at $\gamma t \sim 1.945$ in this case of small σ.

For large σ, the super-radiance effect disappears and N_4 reduces to the independent-atom result,

$$N_4(t) \cong \left(1-e^{-\gamma t}\right)^2$$

Without super-radiance, N_4 reaches 90 % at $\gamma t \sim 2.96$, so the emission occurs more slowly.

This treatment does not yet give a conclusive prediction about the possibility of observation of super-radiance in X-FEL irradiation experiments. Further work is underway as well as discussion of a possible experimental techmique to observe super-radiant emission and distinguish it from spontaneous fluorescence and/or stimulated emission.

REFERENCES

1.) R. H. Dicke, "Coherence in Spontaneous Radiation Processes", Phys. Rev. **93**, 99 (1954).

2.) C. Cohen-Tannoudji, J. Dupont-Roc and G. Grynberg, **Processus d'Interaction entre photons et atomes**, Editions du CNRS, 1988.

3.) R. Rohlsberger, K. Schlage, B. Sahoo, S. Couet and R. Ruffer, "Collective Lamb Shift in Single-Photon Superradiance", Science **328**, 1248 (2010).

4.) R. Rohlsberger, H.-C. Wille, K. Schlage, B. Sahoo, Nature **482**, 199 (2012).

5.) M. Gross and S. Haroche, Physics Reports **93**, 301 (1982).

Appendix C.) Schroedinger equation for a many-atom system

Molecular dynamics (MD) is based on classical mechanics for atomic motion and the atomic kinetics (CR or Collisional-radiative) makes an assumption equivalent to assuming the atomic state is measured on every time-step. This assumption is usual in atomic spectroscopy but it neglects a class of quantum atomic interference effects. The question we want to ask is whether a more rigorous calculation too demanding for normal workstation computers.

For this purpose an existing one-atom Schroedinger equation code[1,2] was converted into a many-atom code[3]. The combined code was used for a test-calculation of the Stark profile of hydrogen atoms moving in the presence of a singly-charged Fe impurity. The calculation was appropriate to a gas of atmospheric density at a temperature of ~ 0.5 eV. Because the hydrogen atoms move with thermal velocities ~ 6 10^5 cm/sec, they experience time-dependent electric fields $\mathbf{E}(\mathbf{R}_j, t)$, where $\mathbf{R}_j(t)$ is the position of the j^{th} hydrogen atom. The calculation we have performed illustrates the kind of calculation that can be performed by a many-atom Schroedinger code (and not easily performed otherwise).

This method can treat physics problems not within the reach of the normal CR method. One effect of this type is the effect of collisions on Doppler profiles[1]. In the CR description the emission is instantaneous and then each emitting atom has a Doppler shift determined by the instantaneous velocity of the emitter. In quantum mechanics, the emission occurs over a relatively long time and the emitting atom (ion) can change velocity or change environment during that time. In that case there can be a complicated frequency modulation of the emission line. A similar effect is possible for emission by many-electron high-Z ions: such ions could change excitation state within the cluster of states forming an UTA during emission. This kind of effect could possibly change the x-ray opacity of dense plasmas and deserves careful analysis for that reason.

Schroedinger equation and line profile:

Our code solves the time-dependent Schroedinger equation for the evolution operator U(t), which generates a time-dependent wave-function

$$\psi(t) = U(t)\,\psi_0 \qquad (1)$$

If the total Hamiltonian H were independent of time, the evolution operator would be

$$U(t) = \exp(-iHt/\hbar) \qquad (2)$$

When H = H(t) contains time-dependent electric or magnetic fields U(t) is found by solving the Schroedinger equation in matrix form:

$$i\hbar\frac{d}{dt}U(t) = H(t)\circ U(t) \qquad (3)$$

From the solution we form the auto-correlation function of the emitting dipole:

$$\Phi_x(t) = Tr\left[\hat{x}\,\hat{U}^+(t)\;\hat{x}\,\hat{U}(t)\;\hat{\rho}_o\right] = \langle \hat{x}(0)\,\hat{x}(t)\rangle \qquad (4)$$

where x is the electron position operator (and likewise for y, z coordinates). The initial density matrix ρ_0 is chosen to put one electron in the 3s-3p-3d set of states (the density-matrix calculation averages all 9 possibilities).

For an observer looking from the y-direction, the emission line profile has the form

$$P(\omega) = \frac{2e^2\omega^4}{3c^3}\mathrm{Re}\int_0^\infty e^{j\omega t}\; e^{-\lambda t}\left[\Phi_x(t)+\Phi_z(t)\right]\,dt \qquad (5)$$

λ is an artificial damping which makes a Lorentz line profile (typically $\lambda = 3\ 10^{11}$/sec in our calculations). Eqs. (4-5) are the standard theory of line-profiles due to Kubo[3], Anderson[4] and Baranger[5] and summarized in textbooks of plasma spectroscopy[6,7].

Atomic states, atomic data

The one-electron basis states are hydrogenic wave-functions,

$$\phi_{n,\ell,m,\sigma}$$

We work with the amplitudes of these basis states but do not directly use the wave functions $\phi_{nlm\sigma}(r)$. We consider the hydrogen 3 --> 2 transitions ("Balmer alpha" lines).

The code can use large and small sets of states:
Large set (60 states): 1s, 2s,2p, 3s,3p,3d, 4s,4p,4d,4f, including spin states
Small set (13 states): 2s,2p, 3s,3p,3d, spin is ignored
For the calculation described here only the small set is used.

The Hamiltonian includes the effect of time-dependent or dynamical electromagnetic fields:

$$H_d(t) = -\boldsymbol{\mu}\cdot\mathbf{B}(t) - e\mathbf{r}\cdot\mathbf{E}(t) \qquad \boldsymbol{\mu} = \mu_o\mathbf{L} + 2\mu_o\,\mathbf{s}$$

This equation omits the "anomalous g-factor" of the electron, a small (0.1%) correction to the factor 2 in the spin moment. The omission is consistent with leaving out the Lamb shift.
If we were only interested in constant fields, it would be most efficient to simply diagonalize the Hamiltonian and find the spectrum. If we were only interested in sinusoidal electromagnetic fields it would be natural to use the Floquet method, which exploits the periodicity of the Hamiltonian by solving only for the time-dependence in one cycle of the field. In our case the time-dependent electric field is the field of one charged impurity at the center of the simulation box; the field is time-dependent as seen by a moving radiator atom.

The code requires the position operators X, Y, Z and angular momentum operators **L**, **S**. For polarization phenomena we even care about the signs, and it is not completely satisfactory to take formulas from books. The well-known book of Bethe-Salpeter uses special signs for spherical harmonics $Y_{\ell m}$ (for $m < 0$) but has a typographical error for the sign of the radial matrix-

element $R_{n,\ell}^{n,\ell+1}$ (See Eq. (63.5)). The textbook of Landau-Lifshitz does not give all the needed formulas. We use the Gordon formula for radial matrix-elements of **r** , correct the sign for n = n', adopt Landau-Lifshitz signs for $\langle n,\ell,m \mid \mathbf{R} \mid n',\ell',m' \rangle$ and modify the Landau-Lifshitz formula for $\langle n,\ell \parallel \mathbf{R} \parallel n'\ell' \rangle$; for safety the matrix commutation relations have been checked for consistency.

In the calculations described here, the MD motion is straight-line motion with periodic boundary conditions inside a 50 Angstrom simulation box. (The box size is small compared to the mean free path at air density.) Each atom moves independently after being launched with random position and velocity. The atoms experience the electric field of an impurity located at the box center; the distribution function W(F) for these electric fields looks very much like the usual Holtsmark distribution. Special provision keeps the atoms from approaching the central impurity charge too closely.

In the usual calculation of line broadening, the line profile for a constant electric field F is averaged against the distribution W(F). In our calculation the field is dynamically changing as the atom moves and the Stark effect responds fully quantum-mechanically to changes in the magnitude and direction of F.

Computer requirements

We follow the time evolution for 60 psec to resolve the Balmer Stark splittings. We use a small time-step $dt \sim 2\ 10^{-17}$ seconds to resolve the characteristic time-evolution of the 2s electron. That means the code must take 1.5 million time-steps.

Eq. (3) is solved by a second-order difference scheme patterned on Simpson's rule. Unitarity of U(t) is used as a test of the calculation. In our calculation, U has errors ~ 0.03 % at the end of a typical calculation. To obtain second-order accuracy, several matrix-multiplications are needed for each time-step. For a 60x60 Hamiltonian, each matrix multiplication requires 216,000 complex arithmetic operations.
The data storage can be seen by the following itemization: storage used for atomic data and matrices: 33 matrices of 60x60; the MD uses N_{at} x 4 more 60x60 matrices.

This method of calculation was described in reference 8 but at that time no calculations had been performed. Results of the first calculations performed in this project are described in section 8 of the main text.

REFERENCES

(1.) D. Burgess, D. Everett and R. Lee, J. Phys **B12**, L755 (1979).

(2.) "Electromagnetic Waves", R. More, T. Kato, Y.S. Kim and M. G. Baik, Chapter 13 in **Plasma Polarization Spectroscopy**, Ed. by T. Fujimoto and A. Iwamae, Springer, Berlin, (2008).

(3.) R. Kubo, in **Many-Body Theory,** Tokyo Summer Lectures in Theoretical Physics, Part 1, Syokabo (Tokyo) and Benjamin (New York), 1966.

(4.) P. W. Anderson, Phys. Rev. 76, 647 (1949).

(5.) M. Baranger Phys. Rev. **112**, 855 (1958); A. C. Kolb and H. R. Griem, Phys. Rev. **111**, 514 (1958);

(6.) H. R. Griem, **Principles of Plasma Spectroscopy**, Cambridge University Press, Cambridge, 1997;

(7.) T. Fujimoto, **Plasma Spectroscopy**, Clarendon Press, Oxford, 2004.

(8) R. More and F. Wang, "**Molecular dynamics with atomic transitions and nuclear reactions**", 24th IUPAP Conference on Computational Physics (IUPAP-CCP 2013), Journal of Physics Conference Series **454**, 012027 (2013).

Appendix D.) Electrostatics

When we consider the geometry of X-FEL target interaction, a question arises about the electrical neutrality of the Fe target plasma. The X-ray FEL pulse ($\sim 2\ 10^{10}$ photons) can ionize K-shell electrons from every atom in a tube of diameter ~ 50 nm through a 10 or 20 micron target foil. The K-shell holes are refilled producing Auger electrons with energies up to 7 keV which have ranges ~ 1 micron, so it is possible to worry that the focal spot charges to a high potential.

A simple estimate based on the number of atoms in the interaction region (approximately $\sim 3\ 10^9$) would imply a high voltage ~ 10 keV. That would be sufficient to confine any subsequently emitted electrons.

If this were correct, it would have implications for the atomic model: energetic electrons could affect the inner-shell populations through collisional excitation and ionization. However, if the energetic electrons freely leave the focal-spot, then collisional excitation/ionization phenomena are not important for the first generation of calculations.

Fe metal is a conductor with a measured resistivity $\rho \sim 10$ μOhm-cm at room temperature. The resistivity increases with temperature (Eq. D-4 gives a curve-fit to handbook data). The conduction time-constant ($= \rho/4\pi$) for Fe is $\sim 8.8\ 10^{-19}$ sec, and this implies that any small non-neutral region is neutralized by a return current in a very short time.

The return-current neutralization can be estimated by considering the focal spot to be a small cylinder of length L and radius R which charges at a constant rate $a = Q_o/t_o$. Q_o is the total charge from ionizing each ion ($Q_o \sim 3.3\ 10^9$ e, where e is the electron charge) and t_o is the X-FEL pulse length ($t_o \sim 10$ fsec).

The total charge of the cylinder at time t is Q(t) and this makes an electric field

$$E(r, t) = 2Q(t) / RL \qquad \text{(D-1)}$$

at the radius of the cylinder. (We neglect small corrections at the ends of the cylinder.) That electric field draws a current $j = \sigma E$ which tends to neutralize the charge Q(t) as it grows (the conductivity $\sigma = 1/\rho$). [Eq. (D-1) uses Gaussian cgs units out of respect for the fact that the equation is a direct application of Gauss's law.]

The rate of change of Q(t) combines charging during the X-ray pulse and the neutralization current

$$dQ/dt = +a - (4\pi R^2)j(R, t) = a - 4\pi\sigma Q(t) \qquad \text{(D-2)}$$

This differential equation is easily solved,

$$Q(t) = \frac{a}{4\pi\sigma}\left(1 - e^{-4\pi\sigma t}\right) \qquad \text{(D-3)}$$

It is clear that if the naive charging $Q^0(t) = a\ t$ would make a 10 keV potential, the return current reduces this voltage to something like 10 volts.

(This argument is a special case of a general theorem given in the textbook of Panofsky and Phillips, section 7-4; MKS units are used there.)

The return current can heat metal outside the x-ray interaction region. In fact, the conductivity and resistivity are temperature-dependent. We curve-fit the values given in the Handbook of Chemistry and Physics:

$$\rho\ [\mu\Omega\text{-cm}] = 3.116 - 3.880\ 10^{-3}\ T[K] + 8.92\ 10^{-5}\ T^2 \qquad \text{(D-4)}$$

Eq. (D-4) gives the resistivity in μΩ-cm as a function of the temperature in Kelvin, and is good up to 800 K. For this range of temperatures, the time-constant is short enough that we do not need to worry about high voltages around the focal spot, but if the temperature were much hotter the situation could be more interesting.

There certainly could be interesting electrostatic effects around the focal spot in an insulator. Probably these would cause a breakdown current (discharge) inside the material. For a transparent insulator, the breakdown could generate a visible light flash that might be an interesting diagnostic. The apparent size of the emitting region would indicate of the range of Auger electrons and might provide an indirect measurement of the voltage and current profiles.

Reference

W. Panofsky and M. Phillips, **Classical Electricity and Magnetism**, 2nd Ed., Addison-Wesley Publishing Co., Reading, Mass., 1962.